



Structures of the cyanobacterial nitrogen regulators NtcA and PipX complexed to DNA shed light on DNA binding by NtcA and implicate PipX in the recruitment of RNA polymerase

Alicia Forcada-Nadal ^{1,2}, Sirine Bibak³, Paloma Salinas³, Asunción Contreras ³,
Vicente Rubio ^{1,2,*}, José L. Llácer ^{1,2,*}

¹Instituto de Biomedicina de Valencia of the CSIC (IBV-CSIC), E-46010, Valencia, Spain

²Group 739 at the IBV-CSIC of the Centro de Investigación Biomédica en Red en Enfermedades Raras of the Instituto de Salud Carlos III (CIBERER-ISCIII), E-28029, Spain

³Departamento de Fisiología, Genética y Microbiología, Universidad de Alicante, E-03690, San Vicente del Raspeig, Spain

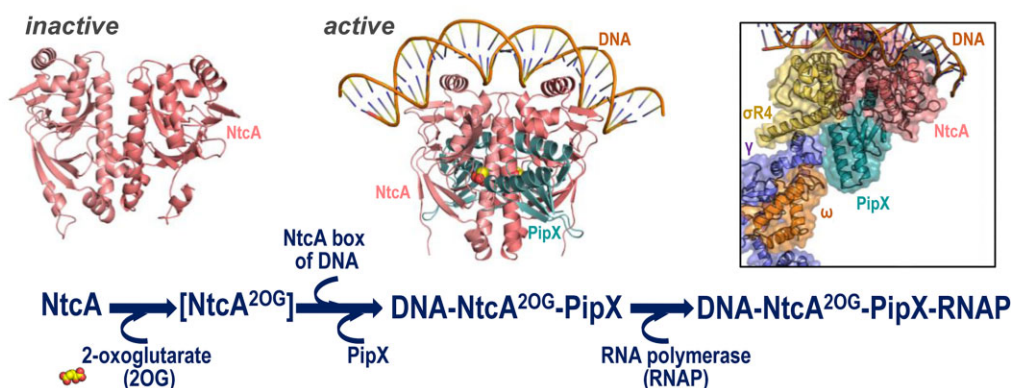
*To whom correspondence should be addressed. Email: jlacer@ibv.csic.es

Correspondence may also be addressed to Vicente Rubio. Email: rubio@ibv.csic.es

Abstract

The CRP-FNR (cAMP receptor protein-fumarate/nitrate reductase regulator) superfamily of transcriptional regulators includes the cyanobacterial master regulator NtcA, which orchestrates large responses of cyanobacteria to nitrogen scarcity. NtcA uses as allosteric activator 2-oxoglutarate (2OG), a signal of nitrogen poorness and carbon richness, and binds a co-activating protein (PipX) that shuttles between the signaling protein PII and NtcA depending on nitrogen richness, thus connecting PII signaling and gene expression regulation. Here, combining structural (X-ray crystallography of six types of crystals including NtcA complexes with DNA, 2OG, and PipX), modeling, and functional [electrophoretic mobility shift assays and bacterial two-hybrid (BACTH)] studies, we clarify the reasons for the exquisite specificity for the binding of NtcA to its target DNA, its mechanisms of activation by 2OG, and its co-activation by PipX. Our crystal structures of PipX–NtcA–DNA complexes prove that PipX does not interact with DNA, although it increases NtcA–DNA contacts, and that it stabilizes the active, DNA-binding-competent conformation of NtcA. Superimposition of this complex on a very recently reported cryo-electron microscopy structure of NtcA in a transcription activity complex with RNA polymerase (RNAP), shows that PipX binding helps recruit RNAP by PipX interaction with RNAP, particularly with its gamma and sigma (region 4) subunits, a structural prediction supported here by BACTH experiments.

Graphical abstract



Introduction

Regulation of gene expression is a crucial process for adaptation of bacteria to changing environments, colonization of diverse niches, and pathogenicity. Key players in these pro-

cesses are transcriptional regulators. Of paramount importance among transcriptional regulators is the superfamily of these proteins known as CRP-FNR (cAMP receptor protein-fumarate/nitrate reductase regulator), which encompasses at

Received: October 14, 2024. Revised: January 22, 2025. Editorial Decision: January 31, 2025. Accepted: February 4, 2025

© The Author(s) 2025. Published by Oxford University Press on behalf of Nucleic Acids Research.

This is an Open Access article distributed under the terms of the Creative Commons Attribution-NonCommercial License

(<https://creativecommons.org/licenses/by-nc/4.0/>), which permits non-commercial re-use, distribution, and reproduction in any medium, provided the original work is properly cited. For commercial re-use, please contact reprints@oup.com for reprints and translation rights for reprints. All other

permissions can be obtained through our RightsLink service via the Permissions link on the article page on our site—for further information please contact journals.permissions@oup.com.

least 21 subclasses and is represented in most bacterial phyla [1, 2]. The members of this superfamily are homodimers composed of an N-terminal dimerization and effector-binding domain (EBD) and of a C-terminal DNA-binding domain (DBD) with a helix-turn-helix (HTH) motif. Members of this superfamily regulate a broad range of processes, including responses to hunger, oxygen, carbon monoxide, oxidative stress, nitrogen fixation, availability to metabolically active nitrogen forms, and photosynthesis [1, 3, 4].

CRP is considered the paradigm for this superfamily and has reached textbook-example status [5]. The determination, more than 30 yr ago, of the crystal structure of CRP bound to its target DNA revealed determinants involved in the specificity of DNA sequence recognition [6]. DNA binding involved the insertion of the α F helices of the HTH motif from each subunit of the CRP dimer into adjacent major grooves of the double-stranded DNA. CRP binding induced a significant bend on the DNA, which was found to facilitate transcription activation [6–11].

DNA binding and transcriptional regulation mechanisms appear to be shared by the members of the CRP-FNR superfamily. However, structural snapshots for protein–DNA complexes have been obtained in just a few cases [12–15]. There is even less information concerning transcription activation complexes (TACs), which include the RNA polymerase (RNAP) holoenzyme. Such information is critical for understanding transcriptional regulation. A crystal structure of the bacterial class II TAC from *Thermus thermophilus* revealed how the CRP/FNR activator TAP enhances transcription initiation through stabilizing interactions with RNAP [16]. Cryo-electron microscopy (cryo-EM) studies of *Escherichia coli* CRP–TAC complexes of class I [17] and class II [18] types have illustrated diverse interactions between CRP and RNAP, offering detailed views of how CRP binding to DNA facilitates transcription by RNAP. Very recently, cryo-EM structures of *Anabaena* sp. PCC7120 TAC with the NtcA master regulator of cyanobacteria (a CRP/FNR superfamily member) have provided additional information on relevant interactions and on cooperative transcription activation by NtcA and the LysR-like regulator NtcB [19].

NtcA, a central subject of this work, is a global nitrogen regulator conserved in cyanobacteria that controls a very large regulon mainly involved in nitrogen assimilation [4, 20–25]. NtcA binds 2-oxoglutarate (2OG), a small molecule that signals the intracellular carbon/nitrogen balance (high levels when carbon is abundant and there is poorness of metabolizable nitrogen [26]) and induces the active conformation of NtcA, binding at a topologically equivalent site to that of cAMP in CRP [27, 28] (Fig. 1). However, NtcA is unique within the CRP/FNR family because it is co-activated by PipX, a small protein conserved in cyanobacteria [29, 30] that shuttles between the carbon/nitrogen/energy sensor/signaling protein PII and NtcA, depending on whether nitrogen richness is high or low [31–34], thus enabling control by PII of gene expression in cyanobacteria [27] (Fig. 1).

We previously [27] determined a crystal structure of NtcA bound to PipX and proposed that PipX would stabilize the NtcA conformation that is competent for binding to target DNA (NtcA box). This box is an imperfect palindrome with three symmetrical specificity-conferring base pairs located 5–7 nucleotides upstream and downstream from the palindrome center [35]. Unfortunately, we were unable to obtain an experimental structure of the NtcA–DNA complex, and, there-

fore, this proposal was speculative, as it was, too, our proposal that PipX, by interacting with RNAP, could help recruit this polymerase to the NtcA-binding site in DNA [27]. The recent structures of the NtcA TAC at the *nirA* promoter [19] offer significant insights but provide no information on NtcA-binding specificity or on the role of PipX.

Here, we define the structural determinants of NtcA binding to target DNA by providing a 3-Å-resolution crystallographic structure of the NtcA of *Synechococcus elongatus* strain PCC7942 bound to both DNA and 2OG. We also present a crystal structure of the quaternary complex of NtcA with PipX, 2OG, and DNA, showing that PipX, without contacting promoter DNA sequences, substantially enhances the binding of NtcA to its target site. We also confirm our previous proposal that PipX binding freezes NtcA in its DNA binding-competent conformation. Importantly, by modeling our PipX–NtcA–DNA complex onto the NtcA–TAC structure (PDB file 8H40) from [19] (a structure that did not contain PipX), and by subsequently testing the interactions between PipX and relevant domains of the sigma and gamma subunits of RNAP in the bacterial two-hybrid system (BACTH), we strongly support that, indeed, PipX enhances NtcA-specific transcription by contributing to the recruitment of the RNAP to the NtcA-binding sites in DNA.

Thus, our work, in addition to defining in great structural detail the determinants of promoter selectivity of NtcA, expands the repertoire of mechanisms of transcriptional regulation, calling attention to the PipX co-activator protein, a specific regulator of cyanobacteria with no known functional counterparts in other taxonomic groups.

Materials and methods

Production and crystallization of NtcA–DNA and PipX–NtcA–DNA and of NtcA in inactive apo forms

NtcA and PipX from *S. elongatus* (strain PCC7942) with N-terminal His₆ tags were produced in *E. coli* Rosetta (DE3) cells (from Novagen) from plasmids pTrc99A-*pipX* and pET15b-NtcA, respectively, and were purified essentially as reported [27, 31]. To produce the V187E mutant form of NtcA, site-directed mutagenesis of the pET15b-NtcA plasmid was carried out using the QuickChange II system (from Stratagene, La Jolla, CA), following the manufacturer's instructions, and utilizing the oligonucleotide pair 5'TCGGCTCAACGCGGGAGACAGTGACG3' and 5'CGTCACTGTCTCCCGCGTTGAGCCGATCG3'. After corroborating by DNA sequencing the introduction of the mutation, the NtcA mutant was expressed and purified as the corresponding wild-type protein.

The DNA used in the crystallization of the NtcA–2OG–DNA complex was prepared by 10-min heating at 65°C of an equimolar mixture of the synthetic oligodeoxyribonucleotides 5'AGCTGATACATAAAAAT3' and 5'CATT TTTTATGTATC3' (from Sigma) in 5 mM Tris–HCl (pH 7.5), followed by slow cooling to 4°C for annealing. These oligonucleotides include one-half of the NtcA binding site of the *S. elongatus* *glnA* promoter (consensus bases are in bold-type), to produce upon annealing the following chained duplex (underlining and italics are used to differentiate individual oligonucleotides; bold-type demarcates consensus bases in the NtcA box):

5'CATT TTTTAT**GTAT**CAGCTGAT**ACATA**AAAAT3'
3'TAAAAATACATAGTCGACT**ATG**TATTTTAC5'

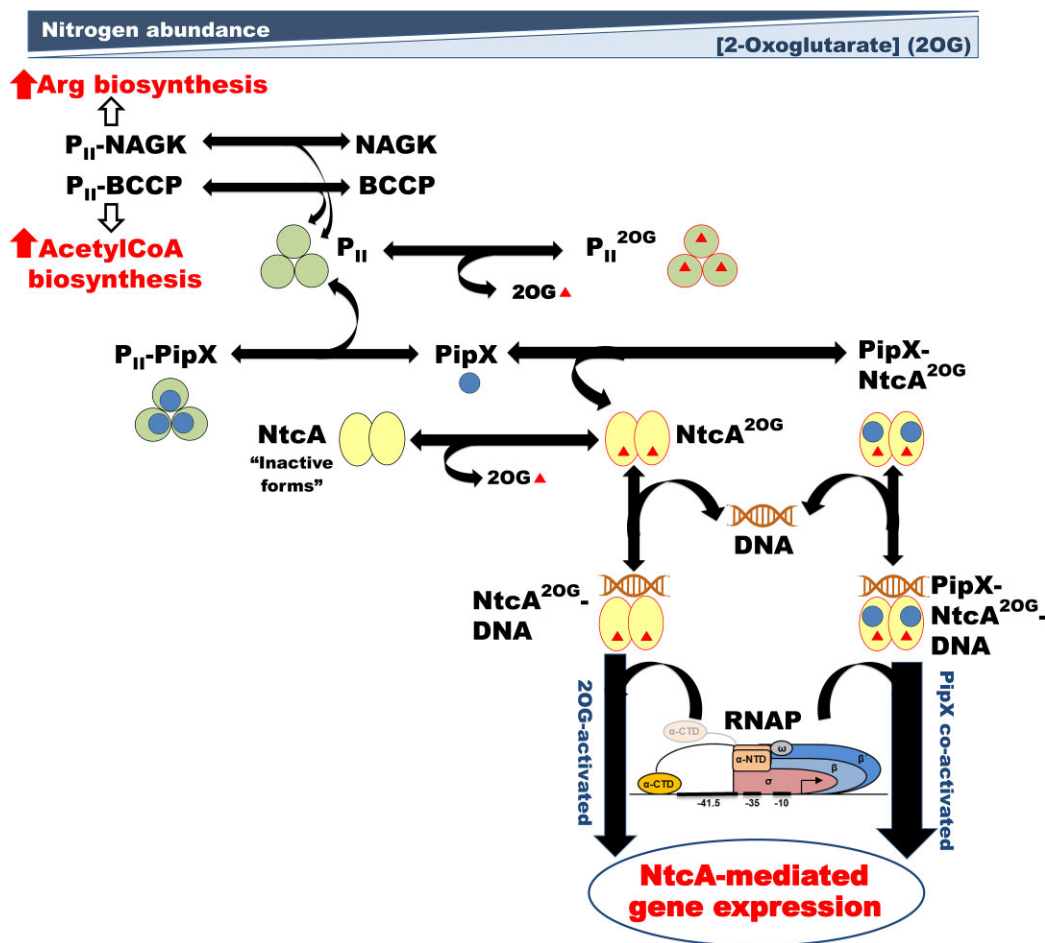


Figure 1. Schematic view of the best-known aspects of the cyanobacterial P_{II}-PipX-NtcA regulatory network, as reference frame for this work. This work provides key crystallographic structural information for “inactive NtcA forms”, and for the active NtcA with DNA alone or in complex with PipX, plus a plausible model for the complex of the ternary complex with RNAP. The DNA is a perfect NtcA box. For further detail see the text as well as our review in [34]. The different thickness of the two bottom arrows symbolizes a higher magnitude of NtcA-mediated gene expression when prompted by PipX-binding to 2OG-activated NtcA, relative to that in the absence of NtcA-bound PipX.

Then, 0.3 mg/ml of this annealed DNA mixture and 0.85 mg/ml NtcA in buffer A [50 mM sodium citrate (pH 6.5), 0.5 M NaCl, 5 mM MgCl₂, 50 mM L-arginine-HCl, 50 mM sodium L-glutamate, and 10 mM 2OG], were incubated for 5 min at 22°C, and concentrated to 7.3 mg protein/ml by ultrafiltration in an Amicon Ultracel YM-50 device. Crystallization sitting drops were prepared by mixing 0.4 µl of the protein-DNA solution and 0.4 µl of crystallization solution. The crystal used was obtained at 21°C in a crystallization solution consisting of 0.1 M Bis-Tris (pH 6.5) and 28% polyethylene glycol (PEG) monomethyl ether 2K.

The procedure to crystallize the PipX-2OG-NtcA-DNA complex was similar to that for the NtcA-DNA complex, although the annealed DNA contained the whole perfect NtcA box (consensus bases are in bold-type) in a symmetric non-cleaved 30-bp DNA duplex with sticky ends (5′ protruding C and 3′ overhanging G in one and the other oligonucleotides) to create the following duplex:

5′CATTTTAT**GTAT**CAGCTG**ATAC**ATAAAAAAT
TAAAAAT**ACATAG**TCGACT**ATGT**ATTTT**AG**5′

We first prepared the NtcA-DNA complex by incubating 0.6 mg/ml of this annealed DNA and 1.4 mg/ml NtcA in buffer A for 10 min at 22°C. Then 0.6 mg/ml PipX was added,

the mixture was incubated for further 10 min and then it was concentrated to ~6 mg protein/ml by centrifugal ultrafiltration. Crystallization sitting drops were prepared as above; after several weeks, two types of crystals were obtained with the following crystallization solutions: crystal type I (0.2 M MgSO₄ and 20% PEG 3350) and crystal type II [0.1 M Tris-HCl (pH 8.5), 2 M ammonium phosphate, and 0.1 M ZnCl₂]. The first crystals obtained of this complex were of type II. They diffracted X-rays at 6-Å resolution, with 63% solvent content. The resolution was improved to 4.3 Å in one crystal by controlled dehydration for 30 min via vapor diffusion versus 50 µl of a solution of 4 M KCl. Initial phases were obtained with this crystal (see below). Then, we obtained crystals of type I that diffracted X-rays up to 3.8-Å resolution.

Crystals of NtcA without 2OG or DNA were obtained in three different forms. They were generated from a 6.1 mg/ml NtcA solution prepared as above except for the omission of 2OG from all solutions and from buffer A. The crystallization solutions were: For form A1 [0.1 M sodium acetate (pH 4.5) and 40% PEG 200]; for form A2 [0.1 M Na-HEPES (pH 6.5) and 20.5% PEG 4K]; and for form B1 [0.05 M Tris-HCl (pH 8), 2 M NaCl, 2% 2-methyl-2,4-pentanediol, 10 mM MgCl₂, and 5% dimethyl sulfoxide].

Data collection and structure determination

Crystals were flash-frozen in liquid N₂. Cryoprotection of crystal II of PipX–NtcA–DNA was as indicated (dehydration) in the previous section. The crystal of NtcA apo form A1 did not need added cryoprotection. All other crystals were cryoprotected by harvesting them in their corresponding crystallization solutions fortified as indicated: for NtcA–DNA, 38% PEG monomethyl ether 2K; for type I crystals of PipX–NtcA–DNA, 39% PEG monomethyl ether 3.35K; and for NtcA apo forms A2 and B1, 25% PEG 400 and 27% 2-methyl-2,4-pentanediol, respectively.

Diffraction was at 100 K in the indicated beamlines (Table 1) of the ESRF or Diamond synchrotrons. Datasets obtained for NtcA A1 and B1, at respective resolutions of 2.70 and 3.33 Å, and for PipX–NtcA–DNA I and II at 3.8 and 4.3-Å resolutions, respectively, were processed and scaled with MOSFLM and SCALA [36] whereas those for NtcA–DNA (3.00-Å resolution) and NtcA apo A2 (2.85 Å) were processed with XDS [37], and prepared with COMBAT [36] for scaling with SCALA. See Table 1 for the space groups and cell dimensions for the different crystals.

Crystallographic phases for the NtcA–DNA crystal (containing also one bound molecule of 2OG per subunit) were determined by molecular replacement with MOLREP [38] using as a model the *S. elongatus* NtcA dimer in its active conformation (PDB file 2XHK; [27]). The initial model was improved by rigid body and maximum likelihood restrained refinement using REFMAC [39]. The phases obtained from this partially refined solution were improved by density modification using program PARROT [40]. An initial model for DNA was manually built using Coot [41]. Then iterative rounds of model building with Coot and refinement with REFMAC and PHENIX [42] were carried out. Tight non-crystallographic symmetry (NCS) restraints were applied until the final rounds of refinement, when they were gradually released. TLS [43] was used in the last steps of refinement, defining the TLS groups after TLS Motion Determination (TLSMD) analysis [44]. All the diffraction data were used throughout the refinement processes, except the 5% randomly selected data for calculating R_{free} . The stereochemical quality of the model was analyzed with MolProbity [45]. The final refined model, at 3.00-Å resolution, contained one NtcA dimer and two chains of each oligodeoxyribonucleotide (Table 1). 2OG was modeled in the NtcA–DNA structure as seen in the active *Anabaena* structure [28].

One subunit of the structure of active NtcA from *S. elongatus* was also used as a model for phasing the dataset for NtcA A1, by molecular replacement with MOLREP. Model building with COOT and refinement with REFMAC and TLS were as for the NtcA–DNA complex. One of the subunits of this final model (which contained two subunits in the asymmetric unit) was used for phasing the dataset for NtcA A2 by molecular replacement using PHASER [46]. A satisfactory solution was found, consisting in one dimer in the asymmetric unit. Model building and refinement were as above to a final resolution of 2.85 Å (Table 1). For NtcA B1, molecular replacement with MOLREP using a subunit of the inactive conformation found previously with NtcA from *S. elongatus* (PDB file 2XKP; [27]) yielded a satisfactory solution, consisting in one subunit in the asymmetric unit, which was refined as with the other datasets, generating a dimer by application of the crystal symmetry.

Crystal II of the PipX–NtcA–DNA complex was originally assigned by XDS to space group I422. From space considerations (Matthew's coefficient calculations; [36]), the asymmetric unit could accommodate one NtcA dimer, one DNA molecule, and two PipX molecules. Initial attempts to find the phases by molecular replacement using the structures of NtcA–DNA (see above) or of PipX–NtcA [27] as searching models failed with both MOLREP and PHASER. We obtained satisfactory phasing solutions by using as searching models either the NtcA dimer alone or the PipX–NtcA complex with only one PipX monomeric molecule. In all these cases, the existence of packing problems in this I422 group for reasonably accommodating a second PipX molecule suggested the possibility of merohedral twinning which would increase the apparent symmetry of the crystal, thus requiring space-group re-evaluation. To assess the twinning of the PipX–NtcA–DNA crystal complex, analyses of the intensity statistics were performed in phenix.xtriage, from the PHENIX software package [42] for an I4 dataset, determining the twin law governing the merohedrally twinned crystal as $(-h, k, -l)$, with a twinning fraction around 0.45 (0.43 or 0.48 for H -test or the maximum likelihood method, respectively). In fact, the use of the dataset for space group I4 instead of I422 only reduced the R_{sym} value from 8.5% to 7.4%, which is another indication of the nearly perfect ($\alpha = 0.5$) merohedral twinning of the crystal. Thus, molecular replacement in space group I4 carried out with PHASER worked with a model composed of one NtcA dimer, one DNA double helical molecule, and one PipX molecule, with Matthew's coefficient of 3.25 Å³ D⁻¹ and 62.2% solvent content. This initial model was subjected to rigid body refinement using REFMAC, applying the twin operator $(-h, k, -l)$ during each round of refinement. Then, and according to the density map, some residues were removed from the model whereas other regions were moved as rigid domains using COOT. The model was finally refined with REFMAC, using the jelly body refinement tool and applying the twin operator $(-h, k, -l)$ during each round of refinement. Local NCS restraints were automatically applied. The final refined model contained in the asymmetric unit two NtcA dimers bound to two DNA duplexes, where one NtcA dimer had two PipX molecules bound as previously reported for the PipX–NtcA dimer [27]. The other NtcA dimer molecule only had one PipX site canonically occupied by one PipX monomer, while the other site contacted aberrantly another PipX molecule from neighboring NtcA₂–PipX₂–DNA complex.

Then, we obtained a dataset for crystal I at 3.8-Å resolution. Analyses of the intensity statistics in phenix.xtriage revealed translational pseudosymmetry. Considering that the resulting symmetry for the initially assigned space group P21 can be defined as P12₁1 by using the universal Herman–Mauguin space-group symbols, molecular replacement was carried out with PHASER in this space group, using as searching assembly the PipX₂–NtcA₂–DNA complex of crystal II, yielding a good solution of two such assemblies in the asymmetric unit, with a Matthew's coefficient of 2.43 Å³ D⁻¹ and 49.5% solvent content. After rigid body refinement with REFMAC, model building in COOT was alternated with a combined refinement using real-space refinement in PHENIX [42] and REFMAC using the jelly body refinement tool. In REFMAC, local NCS restraints were automatically applied. In spite of the limited resolution, both PipX–NtcA–DNA structures (I and II) exhibit very good geometries (Table 1).

Table 1. Data collection and refinement statistics

	Crystals					
	NtcA-DNA	PipX-NtcA-DNA crystal I	PipX-NtcA-DNA crystal II	Apo NtcA form A1	Apo NtcA form A2	Apo NtcA form B1
PBD code	9GUI	9GUK	9GUJ	9GUG	9GQU	9GUH
Beamline (synchrotron)	BM16 (ESRF)	I04.1 (Diamond)	ID23-1 (ESRF)	ID23-1 (ESRF)	BM16 (ESRF)	BM14 (ESRF)
Wavelength, Å	0.9797	0.9173	0.9772	0.9769	0.9797	0.9762
Space group	C2	P12 ₁ 1	I4	C222 ₁	P2 ₁ 2 ₁ 2 ₁	P6 ₄ 22
Unit cell a, b, c (Å)	120.0, 47.0, 139.6	113.3, 68.2, 126.3	165.7, 165.7, 177.6	95.2, 95.5, 160.8	66.5, 88.9, 99.7	96.4, 96.4, 126.9
α, β, γ (°) if $\neq 90$	$\beta = 98.7$	$\beta = 115.1$				
Resolution ^a (Å)	24.2–3.00 (3.16–3.00)	114.4–3.80 (4.01–3.80)	82.9–4.30 (4.53–4.30)	80.4–2.65 (2.79–2.65)	66.3–2.85 (3.00–2.85)	83.5–3.33 (3.51–3.33)
Reflections, total/unique	41 267/15 466	44 255/16 087	59 483/16 116	73 746/21 137	65 283/14 209	36 587/5530
Completeness ^a (%)	98.5 (97.3)	92.2 (86.6)	98.5 (98.5)	98.0 (98.0)	99.0 (95.7)	100 (100)
Multiplicity ^a	2.7 (2.4)	2.8 (2.4)	3.8 (3.7)	3.5 (3.3)	4.6 (3.6)	6.6 (6.9)
I/ σ ^a	7.9 (1.8)	3.0 (1.6)	4.8 (1.6)	5.8 (1.8)	12.1 (2.3)	4.0 (1.8)
CC _{1/2}	0.993 (0.821)	0.983 (0.820)	0.990 (0.793)	0.998 (0.936)	0.999 (0.928)	–
R _{sym} ^a (%)	8.5 (42.9)	19.3 (39.8)	7.4 (47.2)	5.7 (40.8)	5.6 (34.1)	13.6 (41.9)
R _{cryst} /R _{free} (%)	22.7/25.8	30.1/33.8	31.78/33.36	25.5/27.7	23.3/27	23.8/ 27.3
rmsd bond length (Å)	0.011	0.011	0.011	0.010	0.010	0.011
rmsd bond angles (°)	1.54	1.55	1.53	1.69	1.44	1.59
Molecules or atoms/average B-factors (Å ²)						
Polypeptide chains	2	8	7	2	2	1
Protein atoms	3315/65.9	9543/69.5	8108/89.17	2834/91.5	2977/83.4	1657/65.7
2OG	2/51.8	4/55	40/81.2	0	0	0
DNA atoms	1230/81.2	2460/79.7	2419/127.25	0	0	0
Water molecules	4/35.26	0	0	5/64.2	15/57.98	0
Ramachandran plot (%)						
Favored	95.2	96.3	94.6	96	96.2	93.9
Allowed	4.8	3.6	5.27	4	3.5	6.07
Outlier	0	0.09	0.09	0	0.25	0

^aValues in parenthesis are data for the highest resolution shell.

EMSA assay

A fluorescein (Flc)-labeled 159-bp DNA fragment containing the *glnA* gene promoter was generated by polymerase chain reaction (PCR)-amplification with Deep Vent DNA polymerase (New England Biolabs), the primer pair 5'(Flc)CACAACCAGGAAGTGAAGAC3' and 5'(Flc)CGCCTGCAAGATTTTCGTTAC3', and genomic DNA of *S. elongatus* as template. The amplified fragment, purified with GeneClean (MP Biomedicals), was used in gel retardation assays by first incubating 30 ng of this labelled DNA for 10 min at 32°C, in 20 μ l of a solution containing 50 mM HEPES (pH 8), 3 mM MgCl₂, 20% glycerol, 1 mM dithiothreitol, 25 μ g/ml bovine serum albumin, and 0.5 μ g of poly[d(I-C)] (from Roche), and, when indicated, 100 ng of purified NtcA, either wild type or carrying the V187E mutation, and 3.2 mM 2OG. At the end of the incubation the mixtures were subjected to electrophoresis at 120 V for 90 min at 4°C in native 6% polyacrylamide gels in 11 mM Tris-HCl (pH 8), 11 mM Boric acid, and 0.25 mM Ethylene diaminetetraacetic acid (low ionic strength TBE buffer). Experiments were repeated independently in duplicate. Flc fluorescence was visualized using a FUJIFILM-FLA-5000 imaging system.

Modeling of PipX-NtcA-DNA-RNAP transcriptional activator complex

To model the interactions between RNAP and NtcA-bound PipX, we superimposed our PipX-NtcA-DNA complex from crystal I (also done with crystal II; for brevity, given the highly similar results, data here refer to the structure of crystal I,

which is the one with the highest resolution) onto the NtcA-TAC of *Anabaena* (PDB file 8H40) [19]. Our crystal I structure comprises two PipX-NtcA-DNA complexes, with NtcA subunits labeled as A, B, D, and F. Each NtcA subunit from our complex was superimposed onto the NtcA subunit of the NtcA-TAC that is closest to the sigma subunit of RNAP. In each of the four superimpositions, the corresponding PipX coordinates were integrated to generate a PDB file. These PDB files were then analyzed using the PISA server [47] to identify interfacing residues between PipX and the RNAP subunits. The results showed consistent PipX interaction sites, regardless of which NtcA subunit was superimposed. For graphical representations, the superposition of our NtcA subunit F on NtcA subunit X was used. Essentially the same results were obtained when the model was generated by superimposing on the NtcA dimer of the NtcA-TAC structure, one or the other of our two NtcA dimers in our PipX-NtcA-DNA complex of crystal I.

BACTH assays

Strains, plasmids, and oligonucleotides used for this purpose are listed in [Supplementary Table S1](#). Cloning procedures were carried out with *E. coli* XL1-blue, using standard techniques [48]. The construction of BACTH plasmids involved, in brief, the PCR amplification of the relevant coding region, followed by digestion with two enzymes and cloning into the corresponding BACTH vectors previously cut with the same enzymes. A summary is provided in [Supplementary Table S2](#). The correctness of all the constructs was confirmed by automated dideoxy DNA sequencing.

After transformation of *E. coli* BTH101 with pairwise combination of plasmids (50 ng) and subsequent selection on ampicillin (50 $\mu\text{g ml}^{-1}$) and kanamycin (40 $\mu\text{g ml}^{-1}$) LB plates, five clones from each plate were inoculated into 0.5 ml of LB plus antibiotics and 0.5 mM IPTG (isopropyl β -D-1-thiogalactopyranoside) and incubated at 30°C for 24 h. Interactions were assayed by dropping 3 μl of each saturated culture on M63 reporter agar plates containing 0.3% maltose, 0.0001% thiamine, 1 mM magnesium sulfate, 0.5 mM IPTG, and 40 $\mu\text{g ml}^{-1}$ X-gal; and on MacConkey reporter plates containing 1% lactose and 0.5 mM IPTG. Reporter plates were incubated for 24 (MacConkey) or 48 h (M63) at 30°C and photographs were taken at 24 h intervals.

Thermal shift assays

Thermofluor assays [49] were performed using a real-time PCR instrument (CFX Opus 96 Real-Time PCR System, Bio-Rad, Hercules, CA, USA), in tape-sealed 96-well plates, monitoring the change in SYPRO orange fluorescence (excitation and emission wavelengths, 470 and 570 nm, respectively) of 20 μl solutions with the components indicated below, when subjected to an ascending temperature ramp of 1°C/min from 20°C to 80°C. Results are the means of two repetitions on different days of three technical replicates on each experiment. The reaction mixtures (20 μl) contained 0.05 mg/ml ($\sim 1 \mu\text{M}$ homodimer) NtcA, 50 mM HEPES (pH 7.4), 0.15 M NaCl, a 1:1000 dilution of the commercial SYPRO Orange Protein Gel Stain solution (ThermoFisher, catalog number S6651), and, when used, 5 mM of 2OG or of L-glutamate or glutarate (as neutral sodium salts). Controls without NtcA yielded negligible fluorescence changes but their fluorescence profiles were nevertheless subtracted from those of the samples containing NtcA, prior to representation of the thermal profile and sigmoidal fitting using GraphPad Prism 9 (GraphPad Software, San Diego, CA, USA).

Other methods

Protein concentrations were routinely assayed by the method of Bradford [50] using a commercial reagent from Bio-Rad and bovine serum albumin as a standard. Sequence alignments were carried out with Clustal Omega [51], using default values. Superposition of structures was carried out with programs SSM [52] and LSQKAB [36]. Contacts between NtcA and DNA were calculated using PISA [47] or program Contacts [36]. DNA helical parameters were analyzed using w3DNA [53]. Figures of protein structures were generated using Pymol (<http://pymol.sourceforge.net/>).

Results

The structure of the NtcA–DNA–2OG ternary complex

We determined at 3-Å resolution the crystal structure of NtcA bound to its target DNA (Table 1, crystal NtcA–DNA, and Fig. 2A), a palindrome called the NtcA box (consensus sequence, GTAN₈TAC) [35]. For the purpose of crystallization, this box was prepared as a 30 bp DNA duplex incorporating a symmetric motif derived from the first-half of the corresponding box of the *S. elongatus* *glnA* promoter (which is strongly regulated by NtcA) [54, 55] and the preceding nine bases. In this way, a symmetric, synthetic, and expectedly high-

affinity NtcA box was prepared (see below Fig. 2D). To facilitate DNA bending (characteristic for CRP family regulators) this DNA had in each strand a break point between the GTA and TAC parts of the box, with cohesive intervening ends to maintain duplex integrity (see “Materials and methods” section).

In the crystal structure (Table 1, crystal NtcA–DNA) one NtcA homodimer is bound to its target DNA (Fig. 2A). The DBDs of both subunits are wrapped around by a strongly bent ($\sim 80^\circ$) DNA duplex, with the bending largely due to sharp kinks between bases -5 and -6 and 5 and 6 on each side of the dyad axis. In this structure, the protein interacts directly with 20 of the 30 bp of the DNA duplex (Fig. 2A–D), with all the interactions except one (with R29, a residue of the EBD) being mediated by the two DBDs. The major groove of the double helix, hosting in each of two successive turns a half of the palindromic signature sequence, hosts in each turn the initial two turns of the DNA binding helix (helix F) of one subunit or the other subunit of NtcA (Fig. 2B). The axes of the helices are approximately perpendicular to the direction of the DNA chain. In this way, amino acid side-chains emerging radially from each F helix can interact with the surrounding bases and phosphates in each turn of the major groove (Fig. 2B and C). In addition, phosphates in the minor groove of the DNA preceding and following the consensus motif make some contacts with protein amino acids (Fig. 2B and D). The NtcA dimer in this complex closely resembles the NtcA dimer reported previously in the “active” 2OG-bound conformation lacking DNA from *S. elongatus* [27] or from *Anabaena* sp. [28] (rmsd for the superimposition of the dimers, 0.72 Å for 421 C $^\alpha$ atoms or 0.77 Å for 388 C $^\alpha$ atoms, respectively; and see superimposition in Supplementary Fig. S1A). Indeed, our present DNA-bound structure also exhibits the effector 2OG bound on both EBDs via direct and water-mediated hydrogen bonds (inset of Fig. 2A).

Our structure of DNA-bound NtcA is also highly similar to that of the NtcA dimer contained in the recently reported cryo-EM structure of NtcA–TAC complex from *Anabaena*, a complex that also includes DNA [19] (rmsd for the superimposition of the dimers, 2.46 Å for 369 C $^\alpha$ atoms) (Fig. 2E). Actually, our NtcA–DNA complex is also quite similar to the complex of CRP with its target DNA (Supplementary Fig. S1B) (rmsd for the superimposition of 353 C $^\alpha$ atoms with the *E. coli* CRP dimer bound to DNA, 2.69 Å). The reported structures of DNA complexes of other members of the CRP–FNR family are also highly similar (Supplementary Fig. S1C) [7, 12–15], and thus our present results add up to the existing evidence in favor that all members of the CRP transcription factor superfamily activate transcription by binding to DNA essentially in the same way.

NtcA box recognition

The interactions between NtcA and DNA are mediated by residues located in the HTH motif of NtcA, with the specificity being provided by residues of helix αF , which is the one that is inserted in the major groove of DNA (Fig. 2B). Nevertheless, the interactions with phosphate groups of the DNA (Fig. 2B, D) should contribute to the stability of the binding of NtcA to the DNA, but, expectedly, not to the specificity of binding. Particular stabilization is likely to be obtained from ion pairs between the positively charged side-chains of R142,

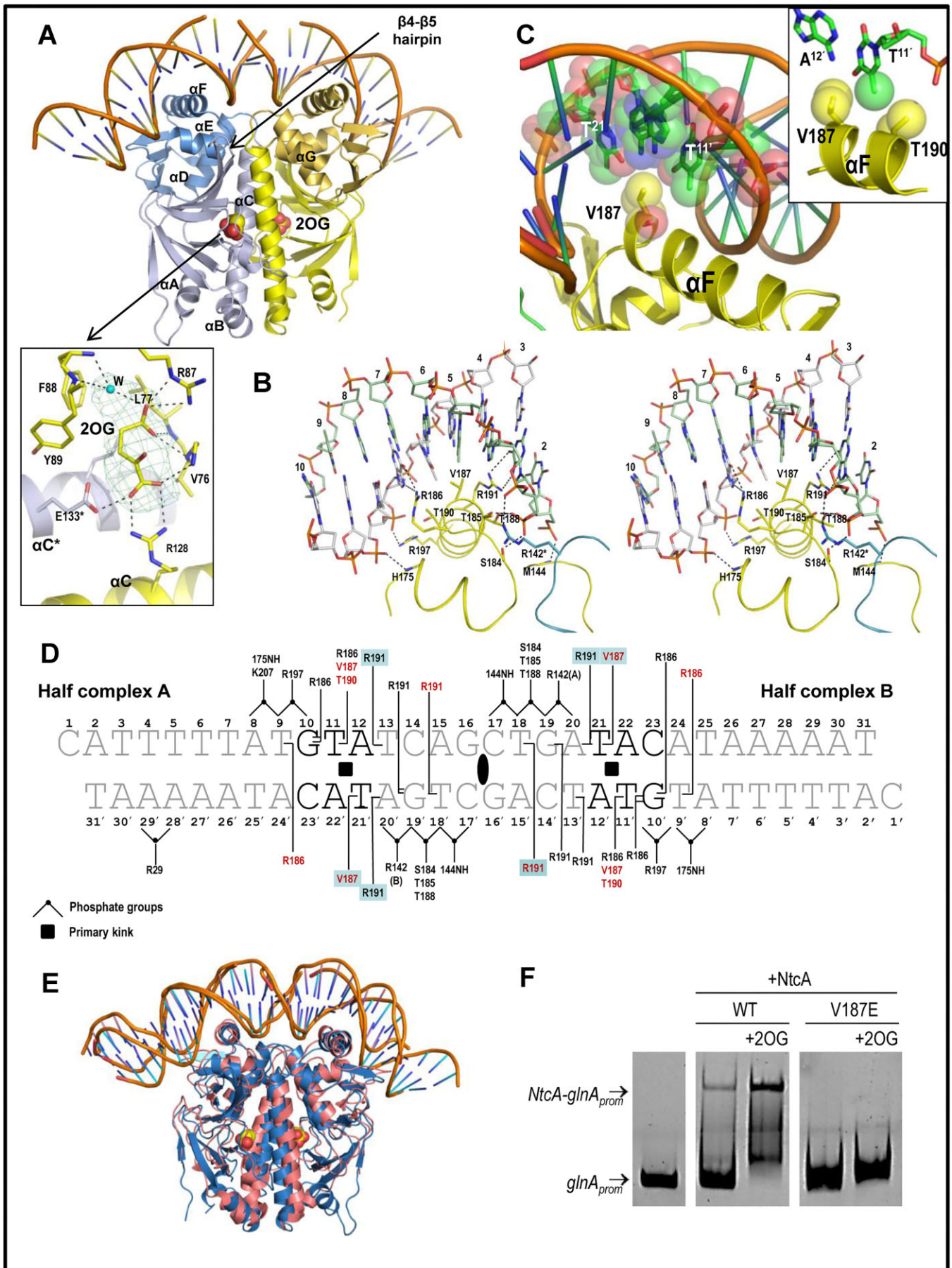


Figure 2. The NtcA-DNA complex structure. **(A)** Overall structure of the complex in ribbons, with bound 2OG shown in spheres representation. Some secondary structure elements of NtcA are labeled. One NtcA subunit is bluish and the other yellow, with the DBD shown in darker hues. The inset

R197 and K207 and the phosphate groups of the DNA (Fig. 2D and [Supplementary Table S3](#)). Particular mention deserves such interaction between R142 and the DNA because, unlike in other members of the CRP family, in which each subunit of the transcription factor exclusively interacts with one half of the DNA consensus sequence, in the case of R142 of NtcA there is cross-interaction with the half of the NtcA box that predominantly interacts with the other subunit of NtcA. Interestingly, the position of R142 (a residue located in the dimerization helix α C) changes depending on the binding or lack of binding of 2OG to NtcA ([27]; and see below). Only in the presence of 2OG is R142 positioned at an appropriate distance to interact with the DNA, while in the absence of 2OG the orientation of α C is such that R142 is too far to make contact with the DNA. Therefore, the indicated (Fig. 2D) interaction of R142 with the DNA phosphate appears particularly important, possibly being a key determinant for enhancing NtcA affinity for its box when 2OG is bound (see Discussion).

As already mentioned, residues of helix F confer specificity to the interaction with the NtcA box, since only four residues of this helix, all of them invariant in the NtcA sequences across cyanobacterial species, R186, V187, T190, and R191, directly contact DNA bases ([Supplementary Table S3](#)). In the cryo-EM structure of the NtcA–TAC of *Anabaena* [19], at least three corresponding residues, R187, V188, and R192, also contact the DNA bases, supporting the importance of these interactions. Two residues, R186 and R191 (numbering for the *S. elongatus* NtcA sequence), form hydrogen bonds with the DNA bases. Thus, the guanidinium group of R186 forms two hydrogen bonds with the O6 and N7 atoms of an invariant G:C pair in the NtcA box, at 7 base pairs from the symmetry axis of the palindrome (Fig. 2B and D). R191 similarly makes hydrogen bonds with the O6 and N7 atoms of a guanine at 3 base pairs from the symmetry axis, outside the conserved bases of the consensus sequence (Fig. 2B and D). These interactions of R191 could contribute to explain the different affinities of NtcA for different promoters that have identical consensus sequences but that show variability in the eight central bases of the palindrome [56, 57]. Massive transcriptomics data [23] identified a G at this position only in ~50% of the putative NtcA promoters of *Anabaena* sp.

Concerning residues V187 and T190, they interact with DNA bases via van der Waals contacts with the methyl group of a thymine (T¹¹ or T^{11'}) at six base pairs from the DNA symmetry axis (Fig. 2B and C and its inset). V187 is particularly

notable for distinguishing NtcA from CRP, being invariant across cyanobacteria, whereas it is replaced by glutamate in CRPs. A mutation substituting V187 by glutamate (as in CRP) abolishes NtcA's ability to bind to its target DNA, as shown in electrophoretic mobility shift assay (EMSA) (Fig. 2F). This underscores the critical role of V187 in NtcA–DNA interaction. The faint but existent retarded band in the absence of 2OG in the EMSA studies with wild-type NtcA, and the absence of this band with the V187E mutant (Fig. 2F) stress the importance of V187 in the binding of NtcA to its DNA box even in the absence of 2OG.

Structures of the PipX–NtcA–2OG–DNA complex

We determined the structure of the quaternary complex of NtcA with DNA, 2OG, and PipX using two types of crystals (crystals I and II) grown under different conditions, and diffracting X-rays at 3.8 and 4.3 Å resolutions, respectively. Unless indicated, we will refer to the structure of crystal I (Fig. 3A–C) since it is the one obtained at the highest resolution (3.8 Å). Crystal I contained in the asymmetric unit (Fig. 3A) two complete PipX–NtcA–DNA complexes in two DNA duplexes chained by the C and G overhangs, totalizing two 30-bp-long DNA molecules hosting two NtcA dimers and four NtcA-bound PipX molecules. Despite the limited resolution, the $R_{\text{factor}}/R_{\text{free}}$ values were quite good (Table 1) and, as illustrated in Fig. 3C, the map had excellent quality, allowing the tracing of most amino acid side-chains, including those at the interfaces between the different components of the complex, what allowed quite detailed mapping of the interactions between the NtcA and DNA.

The two complexes in the asymmetric unit of crystal I are very similar (rmsd of 0.97 Å for 594 superimposed C α atoms). The NtcA dimer and PipX have the same topography and conformation as in the complex of these two components of *S. elongatus* in the absence of DNA [27] (rmsd of 1.04 ± 0.02 Å for 547 ± 1 superimposed C α atoms), with preservation of the PipX–NtcA interactions observed in the PipX–NtcA complex [27]. PipX in this complex adopts the *flexed* conformation (Fig. 3A and B) in which the C-terminal helix (helix B) runs antiparallel to the preceding helix, named A, thus forming a two-helix bundle. The flexed conformation was also found when PipX was not bound to any partner [58] whereas the B helix was extended in at least one of the three PipX molecules trapped in the complex of this protein with PII [27].

details the bound 2OG, modeled as in the NtcA–2OG *Anabaena* structure [28], encased within its electron density omit map contoured at 2.5 σ . Broken lines denote hydrogen bonds with the indicated residues. W: water. (B) Stereo view of the NtcA–DNA interface in one half of the NtcA–DNA complex. NtcA is yellow (except R142 and the loop between α C and α D from the neighbor NtcA subunit, which are bluish). One DNA chain is green and the other chain in gray. Residue side-chains and DNA are in sticks representation, and hydrogen bonds as black broken lines. (C) The DNA and helix F of NtcA, to highlight the complementary van der Waals surfaces and hydrophobic nature of the interactions of the V187 side-chain and of the bases at positions 5 and 6 of the DNA. The inset illustrates the fact that V187 and T190 clamp the methyl group of the thymine base at position 6' of the box, thus endowing it with specificity. (D) Diagram of the NtcA–DNA contacts in the NtcA–DNA and PipX–NtcA–DNA (crystal I) structures. The DNA bases that characterize the consensus NtcA box are highlighted in bold-type. While the majority of the residues shown interact with DNA in both the NtcA–DNA and PipX–NtcA–DNA complexes, those shadowed in blue only interact in the complex that includes PipX. NH144 and NH175 denote that the interactions shown of amino acids 144 and 175 are mediated by the main-chain NH group of these residues. NtcA residues contributing exclusively non-polar contacts are labeled red. The interactions with the bases and with the phosphate groups are differentiated. Double interactions with a base are marked with a double line. R142(A) and R142(B) denote that the interactions are with Arg142 of the other subunit rather than the one providing all other contacts with the B or A moiety of the palindromic target DNA sequence. The black ellipse signals the two-fold symmetry of the palindrome. The black squares mark sites of primary kinks in the DNA. (E) Superposition of the structures of NtcA–DNA (blue, this study) and NtcA–DNA from the NtcA–TAC complex of *Anabaena* (salmon; PDB file 8H40; [19]) to show the great similarity of both structures. (F) Gel retardation assays of biotinylated DNA encompassing the *S. elongatus* *glnA* promoter without (left panel) or with (panels to the right) 100 ng of NtcA either wild type or hosting the V187E mutation, in the absence or, when indicated, in the presence of 3.2 mM 2OG. For details, see “Materials and methods” section.

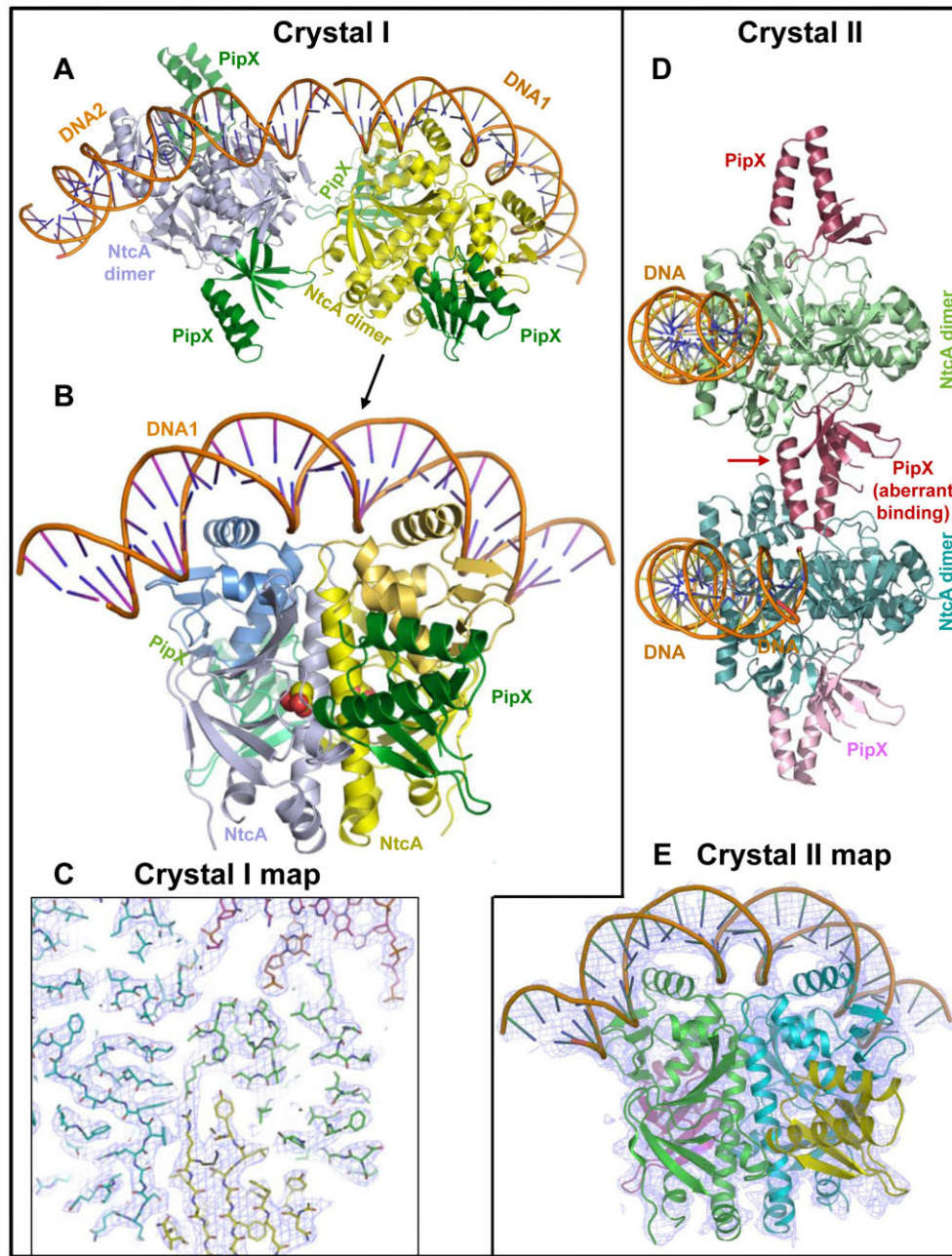


Figure 3. The PipX-NtcA-DNA complexes in crystals I (A–C) and II (D–E). Proteins are in ribbon representation. **(A, D)** Contents of the entire asymmetric units of the corresponding crystals. **(B)** Close-up view of the PipX-NtcA-DNA complex from the crystal at 3.8 Å resolution, with PipX in green. The allosteric effector 2OG is shown in spheres representation (C and O atoms in yellow and red, respectively). **(C)** Illustrative example of the quality of the electron density map. 2Fo-Fc map contoured at 1 σ (blue-violet grid) around the sticks model for DNA (one chain in magenta, the other one in orange) and for PipX (yellow) and NtcA (one subunit cyan and the other one green). **(E)** Close-up view of one complex of crystal II to show the 2Fo-Fc electron density map at 1 σ encircling the model, to illustrate the quality of the map.

DNA is bound as in the NtcA-DNA complex (Fig. 2A), and PipX does not interact with DNA (Fig. 3A). As already mentioned, the interactions of NtcA with the DNA are highly similar to those in the NtcA-2OG-DNA ternary complex, with just three extra interactions made by each NtcA subunit with each half of the palindrome [Fig. 2D (highlighted in blue) and [Supplementary Table S4](#)]. Because of this increase in the number of interactions, PipX might activate NtcA transcription not only by the previously proposed mechanism [27] of stabilizing the “active” conformation of NtcA, but also by increasing the intrinsic affinity of the “active” NtcA dimer for

its target DNA, as shown in surface plasmon resonance experiments [55].

Although the lower resolution of the diffraction data for complex II (Fig. 3D and E) does not favor detailed structural analysis (despite the observation of quite a good map for this resolution, Fig. 3E), the PipX molecules in crystal II (Fig. 3D and E) also have their C-terminal helices flexed and do not contact the DNA, and the individual components in the complexes observed in this crystal are architecturally very similar to the corresponding elements in crystal I and in the PipX-NtcA complex having no DNA bound [27]. For exam-

ple, rmsd values for superimposition of all the PipX molecules in the complexes in crystals I, II, and in the PipX–NtcA complex without DNA [27] were very low (mean of 0.62 ± 0.09 Å for 85 ± 1 C $^{\alpha}$ atoms). Furthermore, the architectures of the PipX–NtcA complexes in crystals I and II are highly similar (rmsd values of 1.00–1.09 Å for 509–594 superimposed C $^{\alpha}$ atoms). Nevertheless, an interesting finding in crystal II was the lack of one PipX molecule. Thus, of the two NtcA dimers bound to DNA, one has two PipX molecules bound as in the complexes observed in crystal I and in the PipX–NtcA complex [27], whereas the other one has one normally bound PipX molecule while the second site for PipX is occupied by the free end of the protruding flexed helices of one of the two PipX molecules of the other dimer (Fig. 3D, labeled “aberrant binding of PipX”). Although this mode of binding may not occur in solution, the complexes in crystal II reveal that NtcA–DNA complexes with canonical [27] occupation of only one PipX site might occur *in vivo*, raising the question of whether the complexes of NtcA with one PipX molecule could differ in efficiency of transcription activation relative to the complex with two PipX molecules bound. As shown below, the existence of a complex with only one molecule of PipX bound would fit the possibility that one PipX molecule could interact with RNAP.

Modeling of PipX–RNAP interactions in the NtcA–TAC complex

To explore the potential existence of interactions between PipX and RNAP in the NtcA–TAC complex if PipX had been present, we superimposed our PipX–NtcA–DNA complex (crystal I) onto the NtcA–TAC structure (PDB file 8H40) [19], following the methodology described in the “Materials and methods” section. The resulting model indicated that PipX could fit into the complex without causing any steric clashes (Fig. 4A–C). The model also shows that only one PipX molecule interacts with the RNAP (Fig. 4A and Supplementary Fig. S2), consistent with the structural observation in our PipX–NtcA–DNA complex (crystal II), where only one PipX molecule is canonically bound to NtcA. This suggests that our observed structure of the complex with only one canonically bound PipX molecule is functionally relevant.

The model predicts that PipX contacts through its C-terminal helices A and B with domain 4 of the sigma subunit (region 4) of RNAP, as well as with the gamma subunit and, to a lesser extent, with the omega subunit (Fig. 4A–C). PISA server analysis predicts that the gamma subunit, via residues I393, R394, S395, G396, M397, and N399, could interact with helix A of PipX (potentially interacting residues of PipX, N55, R58, M59, D62, N63, and R66); that the sigma subunit region 4 (σ R4) could contact via its residues P379, N380, S383, V384, K386, and E387 with PipX helix A (residues R54, N55, and R58) and helix B (residues Q86, T87, F88, and L89), whereas PipX residues R66, R69, and R70 would be positioned near residues S49 and E51 of the omega subunit of the polymerase (Fig. 4C).

Functional evidence for PipX–RNAP interactions provided by BACTH assays

Functional support for PipX interactions with the polymerase was obtained using BACTH assays. The BACTH assays can reveal protein–protein interactions by reconstitution in *E. coli* of the adenylate cyclase of *Bordetella pertussis* [59, 60]. Frag-

ments of the sigma ($\sigma^{319-399}$) and gamma ($\gamma^{374-424}$) subunits predicted to interact with PipX were tested for interactions with PipX and control proteins. Since false negatives are a common issue in two-hybrid assays [61, 62], to maximize possibilities, we constructed N- and C-terminal fusions of $\sigma^{319-399}$ and $\gamma^{374-424}$ fragments to each of the adenylate cyclase domains (T18 and T25), generating eight fusion derivatives that were then tested against previously validated PipX–T25, PipX–T18, T25–PipX, or T18–PipX constructs [61, 62]. To support the specificity and reliability of the interactions, control proteins were also tested against $\sigma^{319-399}$ and $\gamma^{374-424}$ (Supplementary Fig. S3).

As shown in Fig. 4D, this technique provided clear support for the interaction *in vivo* of PipX with portions of the gamma and sigma subunits of RNAP that encompass the residues predicted by our structural modeling to participate in the interactions. In more detail, interaction signals between PipX–T25 and $\sigma^{319-399}$ or $\gamma^{374-424}$ derivatives were obtained in all four tested pairs, while PipX–T18 interacted with T25– $\sigma^{319-399}$ or $\sigma^{319-399}$ –T25. None of the four polymerase fragments gave interaction signals with any of the proteins used as controls (Supplementary Fig. S3), thus supporting the specificity of the interactions observed with PipX. To provide further control for the structural model, we next tested whether deleting the C-terminal helix B of PipX impaired interaction signals from positive PipX/ $\sigma^{319-399}$ or PipX/ $\gamma^{374-424}$ pairs since the prediction from the structural modeling was that three residues of helix B participate in the interactions (see above). As expected, signals were abolished or severely reduced in all cases.

Not surprisingly, false negatives were also obtained amongst some of the relevant and control proteins assayed (Fig. 4D and Supplementary Fig. S3). For instance, T25–NtcA or T18–NtcA failed to interact with $\sigma^{319-399}$, despite direct structural evidence [19] or predictions (this work), suggesting that adding extra domains at the N-terminus of NtcA disrupts the interactions with the corresponding polymerase fragment. The same consideration may apply to PipX since both T25–PipX and T18–PipX gave negative results with the polymerase fragments tested. On the other hand, the failure of PipX–T18 to give interaction signals with $\gamma^{374-424}$ might be attributable to stoichiometric differences, since in this system, due to differences in plasmid-copy numbers, fusions to T18 are systematically expressed at higher levels than fusions to T25 [60]. If that was the case, the implication is that comparatively more $\gamma^{374-424}$ than $\sigma^{319-399}$ would be required to detect interactions with PipX in our assays.

Overall, these BACTH results agree with the predictions made by the structural modeling and provide strong support for the involvement of PipX in direct contacts with specific domains of the RNAP subunits sigma and gamma at NtcA-regulated promoters.

Newly identified NtcA apo forms and NtcA activation by 2OG

NtcA exhibits structural variability depending on its active or inactive state dictated by the presence or absence of 2OG. Active NtcA, either alone or complexed with PipX [27] and DNA (present studies), maintains an essentially constant conformation that closely resembles that of other active Crp/Fnr superfamily members, highlighting a conserved mechanism of activation (Supplementary Fig. S4).

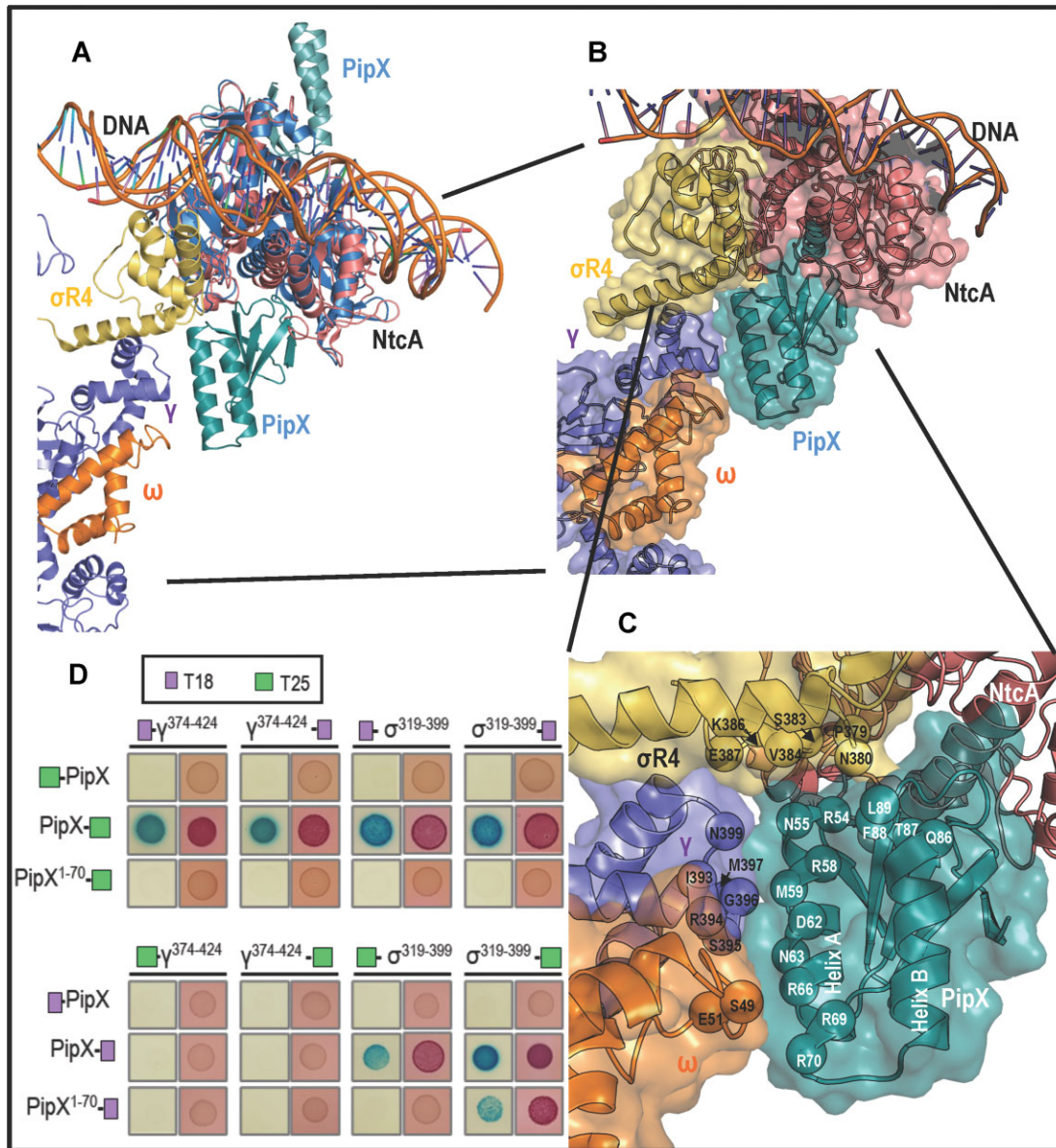


Figure 4. PipX-RNAP interactions. For clarity, only the gamma, omega, and domain 4 of the sigma subunit of RNAP are depicted in all representations. **(A)** Cartoon representation of the model created by superimposing the structure of our PipX-NtcA-DNA complex from *S. elongatus* (crystal I) over the one of the NtcA-TAC complex (PDB file 8H40) of *Anabaena*. The common elements of the two structures (DNA and NtcA dimer) were superimposed with Pymol (<http://pymol.sourceforge.net/>). NtcA dimers are in salmon for *Anabaena* and blue for *S. elongatus*. PipX molecules are blue-cyan and the parts shown of the σ , γ , and ω subunits of RNAP are gold, blue, and orange, respectively. **(B, C)** Close-ups of the NtcA-TAC complex with modeled PipX on the basis of the superimposition in panel (A). Proteins are shown in transparent surface representation to exhibit inside their chain folds in cartoon representation. In panel (C), the zoom is increased to show the PipX-interfacing residues (see "Materials and methods" section) and their positions within the model, alongside the corresponding RNAP-interfacing residues. Amino acids are identified in single-letter code, and the two C-terminal helices A and B of PipX are labeled. **(D)** Interactions between PipX and $\sigma^{319-399}$ or $\gamma^{374-424}$ in the BACTH system involve α -helix B. Experimental evidence using pilot BACTH analyses of PipX interactions with the indicated regions of the gamma and sigma subunits of RNAP ($\sigma^{319-399}$ and $\gamma^{374-424}$), which encompass the residues proposed in panel (C) of this figure to mediate the interactions. The relative position of the T25 or T18 domains of *cyaA*-encoded adenylate cyclase in the indicated chimeras is shown by placing the corresponding domain N- or C-terminally relative to the potentially interacting proteins (identified by their names) before or after the name of the potentially interacting protein. Representative photographs of plate-drop assays corresponding to the indicated pairs of fusion proteins. BTH101 co-transformants were tested in parallel on MacConkey + lactose (right panel) or M63 + maltose + X-gal (left panel) and an average of six assays were performed.

In contrast, the reported “inactive” forms of *Anabaena* NtcA without 2OG [28] (called here form A) or of *S. elongatus* NtcA with aberrantly bound 2OG [27] (called here form B) show significant mutual structural differences (RMSD of 3.67 Å for 306 C α atoms; and see below) where A resembles more the active form than form B. By determining new crystal structures of *S. elongatus* NtcA (Table 1) in the absence of 2OG, we now report three additional inactive conformations which have no 2OG bound (called “apo forms”) (Fig. 5A). Two novel forms (A1 and A2; Fig. 5A and Table 1) resemble but are not identical to the A form reported previously for *Anabaena* NtcA [28] (Supplementary Fig. S5, left-most two and one structures of the 1st and 2nd rows, respectively). These forms exclude that the A-type inactive form were specific for *Anabaena*. The third novel inactive form reported now (form B1; Fig. 5A and Table 1) closely resembles the previously reported [27] inactive form B (Supplementary Fig. S5, the two rightmost structures of the first row), but lacks the aberrantly bound 2OG found in the B form, with important differences with B in the 2OG site, particularly affecting residues 76–78, and 88, having nearly buried the empty 2OG site (Supplementary Fig. S6A). Despite their mutual similarities, forms A1 and A2 presented different crystal packing (C222₁ and P2₁2₁2₁, respectively), as was the case for form B1, which belonged to space group P6₄22 (Table 1).

The comparison of the various inactive conformations of NtcA (epitomized by the structures shown in Fig. 5A) with the highly constant active conformation of this transcriptional regulator hosting correctly bound 2OG (Figs 2A and E, 3B and E, and 4A) shows that 2OG triggers a conformation exhibiting rearrangements in the EBD that propagate throughout the NtcA dimer, significantly impacting the relative positioning of the DNA-binding helices (α F) (Fig. 5B and Supplementary Movie S1). In the active state, the distance between the DNA-interacting helices of the two subunits is short (34.8 Å), aligning perfectly for DNA binding at the two adjacent turns of the NtcA box where they sit (Figs 2A and E and 3B and E). In contrast, these transcriptionally “inactive” forms exhibit changes of orientation and displacements of the F and F* DNA-binding helices of the dimer (the asterisk signals the other subunit of the NtcA homodimer), reflected in increases in their mutual distance (to 37.6, 38.4, and 53.1 Å in form A1, A2, and B1, respectively; Fig. 5A), thus preventing proper interaction of these F helices with DNA for transcriptional activation (Fig. 5B). This alteration is closely tied to shifts in the interfacial α -helices (α Cs), which in active NtcA are close to the two-fold axis of the dimer, forming a true coiled-coil, whereas in inactive forms they diverge more or become more parallel (Fig. 5A and B). Key to these reorientations of the C-helices are 2OG-triggered changes in the interactions across the interface that involve the side-chains of E133 and E137 (Fig. 5C and D and Supplementary Fig. S6B). The changing partners of these two glutamate side-chains depending on whether 2OG is bound or it is not bound, favors the reorientation of the C-helices and, secondarily, of the DBDs, which become poised in a fixed conformation fitting the two turns of the major groove of the double helix in the region of the NtcA box. A critical feature in this structural modulation is the β 4- β 5 hairpin (Fig. 5E).

In the active conformation, the interaction between 2OG and E133 disrupts prior contacts involving R55 and Y89 from the β 4- β 5 hairpin, freeing the latter to adopt a DNA-compatible conformation. Furthermore, this conformational

change may be key to understand the second mechanism, besides increasing promoter affinity, by which 2OG could activate NtcA-dependent transcription, as seen in other family members of class II transcriptional activators such as FNR, CooA, and CRP [5, 63, 64]. The β 4- β 5 hairpin belongs to the region called AR3 (activator region 3), the area of the transcription factor that interacts with the sigma subunit of RNAP in class II TACs. Moreover, in NtcA the conformation of the β 4- β 5 hairpin is also important for the interaction with PipX, since in “active” NtcA, this hairpin interacts with the C-terminal end of the C-terminal helix (helix G) of the neighboring subunit (Fig. 5A), so that the conformation of this helix changes to one suitable for interacting with PipX [27].

An indirect attestation in solution of the occurrence of 2OG-triggered conformational changes in NtcA was the observation of a substantial increase in the thermal stability of NtcA at saturation of 2OG, reflected in thermofluor assays (Supplementary Fig. S6C). These assays showed a substantial shift toward higher temperatures in the fluorescence change associated with thermal unfolding of NtcA when 2OG was added (Supplementary Fig. S6C, compare black with red traces). The specificity of this effect for 2OG was supported by the observation that L-glutamate, which differs from 2OG in the replacement of the keto group by an amine group, had little if any effect on the curve of fluorescence change, whereas glutarate, in which the keto group of 2OG is replaced by two hydrogens, had considerably smaller effect than 2OG (respective T_m values 1°C and 3°C higher than in absence of additions; Supplementary Fig. S6C).

In summary, our results show that NtcA, as other factors of the CRP-FNR superfamily, can adopt multiple transcriptionally inactive conformations (Supplementary Fig. S5) in the absence of its small-molecule allosteric effector (2OG in the case of NtcA), in contrast with the constancy of the active conformation of the transcriptional regulators of this family (Supplementary Fig. S4) [65–71].

Discussion

NtcA activation and DNA binding

Transcription activation by NtcA and other members of the Crp/Fnr superfamily relies on their ability to specifically bind DNA in their active states, followed by subsequent interaction with RNAP [13, 14, 16, 27, 70, 72–75]. NtcA and several related factors target class II activated promoters, where key interactions are centered around 41.5 nucleotides upstream of the transcription start site, facilitating RNAP recruitment and the formation of active transcription complexes [5, 63, 64, 76]. Activation typically involves a rotation of the DBD upon induction, optimizing the arrangement of DNA recognition helices for binding [66, 69]. The binding of the allosteric effector and nitrogen poorness sensor 2OG is crucial for NtcA activation, since it enables specific interactions with the NtcA box that are necessary for effective RNAP recruitment.

Recently, the determination by Cryo-EM of the structure of a NtcA–TAC complex from *Anabaena* [19] has provided insights into how DNA looping facilitates transcription activation by NtcA. DNA looping allows NtcA to bring together distantly located DNA-binding sites, enabling the transcription factor to effectively recruit RNAP and activate transcription in a cooperative manner. However, the overall relatively high resolution (for cryo-EM) of the NtcA–TAC structure (3.6 Å),

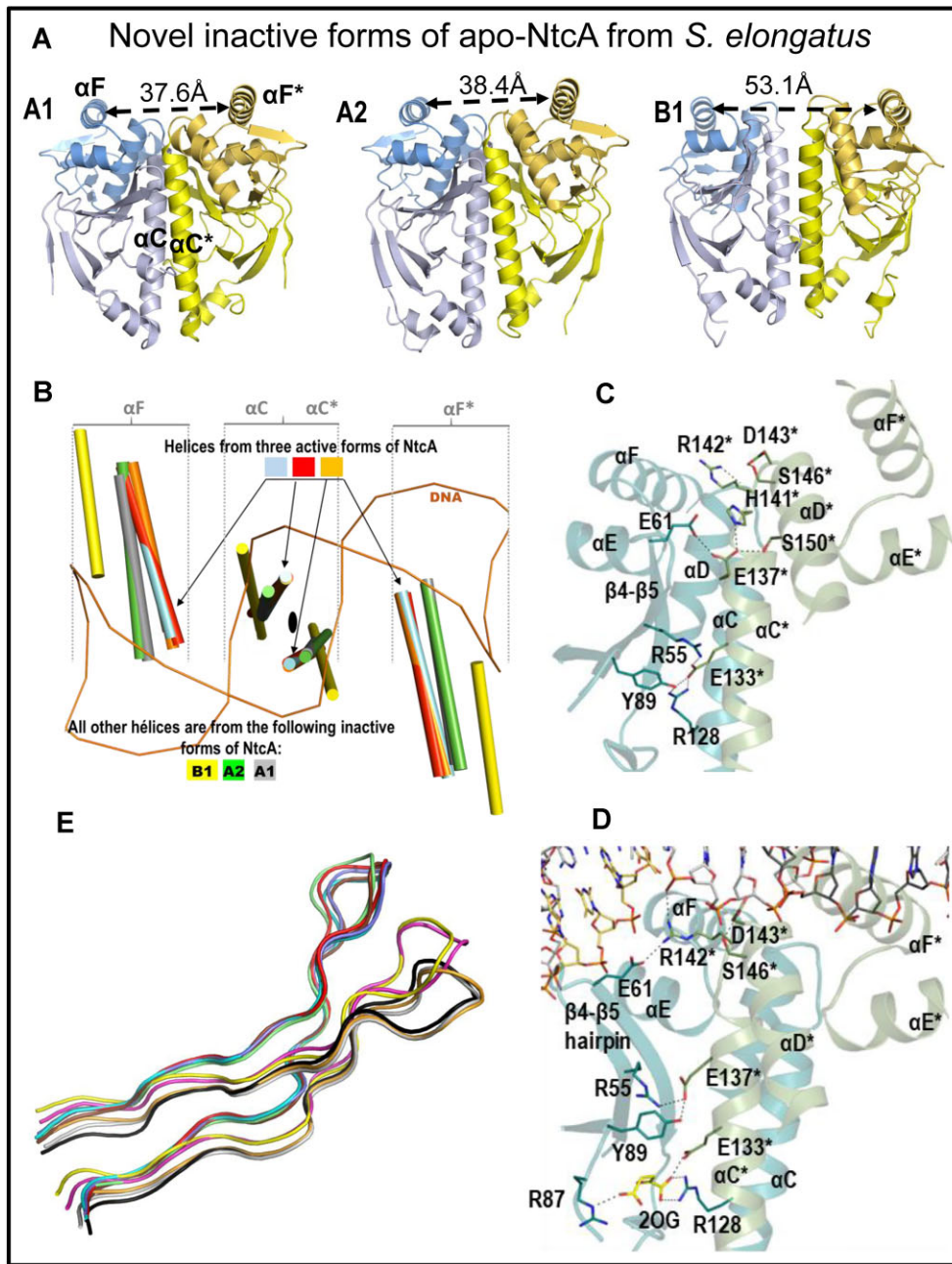


Figure 5. NtcA apo structures and movements of the interfacial helix, the DNA-binding helix, and the $\beta 4-\beta 5$ hairpin upon activation. **(A)** Ribbon representations of NtcA in its novel apo structures, A1, A2, and B1. The distance between the DNA-binding region of the F helices of both subunits are given in \AA over a double-headed broken arrow. The interfacial helices $\alpha C/\alpha C^*$ and the DNA-binding helices $\alpha F/\alpha F^*$ are labeled in the A1 form (top leftmost panel). **(B)** The figure illustrates the movements of the $\alpha C/\alpha C^*$ and $\alpha F/\alpha F^*$ helices, detected by superimposing the different apo or active forms of NtcA. The helices are in cylinder representation, and identified for each NtcA form (code shown in the figure itself). Active forms: NtcA bound to DNA (red), PipX-NtcA-DNA complex (orange), and NtcA-2OG complex (cyan; PDB file 2XHK). Inactive forms: A1 (gray), A2 (green), and B1 (yellow). The αC and αC^* helices (interfacial helices) are oriented almost perpendicularly to the image plane. The backbones of the two strands of the DNA, from the PipX-NtcA-DNA complex, are shown as orange lines. The two-fold axis of NtcA (black ellipse) is perpendicular to the plane of the image. An asterisk (*) distinguishes helices from one subunit versus those of the other. **(C, D)** Mechanism of NtcA activation based on the structures of NtcA A1 **(C)** and NtcA-DNA **(D)** from *S. elongatus*. Ribbon representations showing key residues involved in signal transmission from the 2OG-binding site to the DNA-binding helices. One NtcA subunit is blueish and the other one greenish, with the residues of the latter subunit marked with an asterisk. Hydrogen bonds are depicted as dashed lines. An equivalent projection of inactive form A1 is shown as supplementary material (Supplementary Fig. S5B) to show that changes in essentially the same residues although of different magnitude do occur. **(E)** Comparison of $\beta 4-\beta 5$ hairpin conformation between the active and inactive forms of NtcA. NtcA-DNA (red), PipX-NtcA-DNA (brown), PipX-NtcA (cyan; PDB file 2XKO), NtcA-2OG from *S. elongatus* (blue; PDB file 2XHK), NtcA-2OG from *Anabaena sp.* (green; PDB file 3LA2), NtcA A1 (gray), NtcA A2 (black), NtcA A from *Anabaena sp.* (orange; PDB file 3LA7), NtcA B1 (yellow), and the reported NtcA B from *S. elongatus* in inactive conformation hosting aberrantly bound 2OG (magenta; PDB file 2XKP).

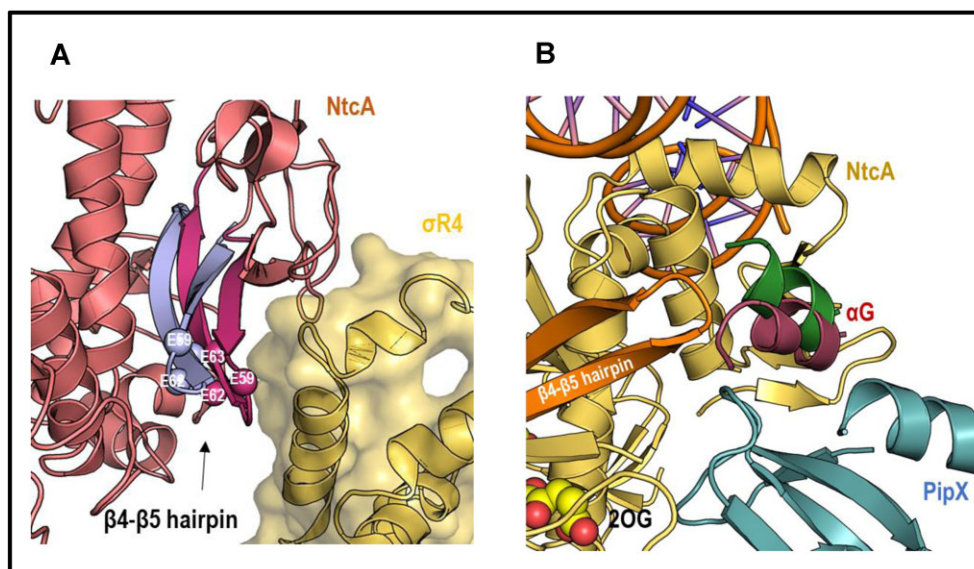


Figure 6. Involvement of movements of the β 4- β 5 hairpin and of helix G of NtcA in the activation of this transcriptional regulator by 2OG. **(A)** Superposition of the NtcA apo A1 structure from *S. elongatus* (this work) onto the NtcA subunit that is closest to the sigma subunit of RNAP in the NtcA-TAC complex (PDB file 8H40), to highlight the conformational change in the β 4- β 5 hairpin of NtcA upon 2OG binding. For clarity, only the sigma subunit domain 4 (yellow) and NtcA (salmon) of NtcA-TAC are shown, also showing (in light blue) the β 4- β 5 hairpin of the A1 structure, whereas the β 4- β 5 hairpin from the NtcA-TAC complex is hot pink. Three hairpin residues that interact with sigma R4 are shown as spheres and are labeled. **(B)** α G helix movement in the PipX-NtcA-DNA complex (α G helix in red) relatively to the inactive NtcA A1 structure (α G helix in green). The β 4- β 5 hairpin of NtcA in the PipX-NtcA-DNA complex is in orange. 2OG is shown in spheres representation.

contrasts with the low local resolution for NtcA and the NtcA box (<5.5 Å), and, therefore, our structure of NtcA bound to its target DNA at 3.0-Å resolution offers unique detail on the specific recognition of the NtcA box.

This recognition is shown here to result from a precise interaction pattern of four residues of the α F helix, Arg186, Val187, Thr190, and Arg191, with a few DNA bases of the NtcA box. These amino acid residues should allow discrimination against other bacterial transcription factors of the same family. This discrimination was previously proven for the closely related transcription factor CRP [55]. Val187, which in CRP is replaced by a glutamate residue, is an important discriminator, since the present structures clearly predict steric and polarity clashes (not shown) in the NtcA-DNA complex if valine was replaced by glutamate. Indeed, such substitution is proven here in EMSA assays to abolish the binding of NtcA to its NtcA box. In addition, our structures also highlight the importance of extensive contacts of NtcA residues (such as Arg29, Met144, His175, Thr185, and Thr188) with phosphate groups of the target DNA. While these interactions are largely shared by CRP, the binding of Arg142 to a phosphate group is restricted to NtcA. Instead of interacting with the DNA adjacent to its subunit, Arg142 interacts with the DNA bound by the other NtcA subunit (Fig. 5D). The double interaction revealed here with a DNA phosphate and with an invariant residue (Glu61) of the β 4- β 5 turn from the regulatory domain (EBD) of the adjacent NtcA subunit endows Arg142 with a key role in the allosteric activation of NtcA by 2OG binding.

The movement of the β 4- β 5 hairpin that crucially differentiates the active and inactive states of NtcA (Fig. 5E) is integral to NtcA function. In this movement, 142 is a key residue at the center of an ion-pair network that connects the DNA with dynamic elements of NtcA like helix C and the β 4- β 5

hairpin (Fig. 5C and D and [Supplementary Fig. S6C](#)). The different conformations of this β hairpin depending on the activation state of NtcA (Fig. 5E) are connected to movements of the HTH DNA binding motif of the same subunit (Fig. 5D). In the inactive forms, interactions between Glu133 from one NtcA subunit and Arg55 from the other subunit promote a different conformation of the β 4- β 5 hairpin that affects the HTH (Fig. 5C and D and [Supplementary Fig. S6C](#)). The β 4- β 5 hairpin is part of the AR3, a region interacting with the sigma subunit of RNAP [5, 63, 64]. In agreement with this assignment, in the NtcA-TAC complex [19], NtcA interacts with σ R4 (Fig. 4A) through Arg39 and glutamate residues 59, 62, and 63 (Fig. 4C), the latter three located in the β 4- β 5 hairpin (Fig. 6A). Superimposition of the inactive NtcA A1 form onto the NtcA-TAC complex highlights the shift of the position of the β 4- β 5 hairpin upon 2OG binding, which moves closest toward the sigma subunit of RNAP, thus strengthening the interaction of NtcA with RNAP (Fig. 6A) and also illustrating why the binding of 2OG activates transcription by NtcA via promotion of effective interaction with RNAP. Interestingly, α G, the C-terminal helix characteristic of NtcA and absent in CRP, mediates some of the interactions of NtcA with PipX [27] and undergoes a positional shift upon 2OG binding to NtcA. This shift should facilitate NtcA interaction with PipX (Fig. 6B), likely contributing to the co-activation process.

Roles of PipX in NtcA-dependent transcriptional regulation

Determination of the structure of the PipX-NtcA-DNA complex has been essential for elucidating the co-activator role of PipX, showing that NtcA and PipX in this complex retain the same conformations as in their binary complex without DNA

[27], and for confirming that PipX is positioned away from the DNA (Fig. 2A, B, and D). Despite its moderate resolution (3.8 Å, crystal I), our data for the PipX-NtcA-DNA complex clearly reveal additional interactions between NtcA and DNA that are absent in the binary NtcA-DNA complex (Fig. 2D). These extra contacts, strengthening the NtcA-DNA interaction, possibly explain part (see below) of the co-activating role of PipX.

Our structure also confirms the stabilization by PipX of the active conformation of NtcA that is promoted by 2OG binding [27], likely another key factor in PipX co-activation. By binding to the active form, PipX shifts the equilibrium between inactive and active form toward the active one. Actually, each PipX molecule interacts with the EBD of one NtcA subunit of the dimer and with the DBD of the other subunit [27], stabilizing the correct orientation of the F helix for DNA binding.

We previously proposed [27] that PipX could also help recruit RNAP to DNA-bound NtcA, since significant portions of the surface of PipX, particularly its two C-terminal helices, remained exposed in the PipX-NtcA complex. This exposition is now confirmed for the structure of PipX-NtcA-DNA. The interaction with RNAP is further supported by our model in which we superimposed the PipX-NtcA-DNA complex structure on that of NtcA-TAC lacking PipX [19], with excellent fitting of all elements including PipX, which is integrated without steric clashes. It is worth noting that, despite methodological differences concerning structural determination (crystallography versus cryo-EM), both structures are highly similar in their common parts, including key regions relevant for transcriptional activation, notably the orientation of NtcA with respect to the DNA. In our modeled supercomplex, supported by BACTH interaction assays, the C-terminal helices of PipX interact with σ R4 of RNAP, as well as with the gamma subunit, and, to lesser extent, with the omega subunit (Fig. 4).

Matching our model, in which a single PipX molecule would be enough for helping recruit RNAP toward NtcA DNA targets, our crystal II structures only had one out of the two possible PipX molecules binding to their NtcA sites (Fig. 3D). The binding of the two PipX molecules to far apart sites at the NtcA dimer should be independent of each other and thus the NtcA₂-PipX₂ and NtcA₂-PipX complexes, as well as NtcA₂ molecules, could be expected to coexist *in vivo*. Since the intracellular levels of PipX appear constant at varying conditions [77], PipX availability to bind NtcA mainly depends on the very abundant protein PII [78] and on the 2OG levels, which inversely affect PipX-PII and PipX-NtcA complexes, and, remarkably, of PII effectors ATP/ADP. The importance of PII-specific effectors for PipX-NtcA complexes have recently been demonstrated by NanoBiT complementation assays showing that changes in ATP levels have a dramatic impact on PipX-NtcA interactions in *S. elongatus* [79]. In any case, the changes in PipX availability could nuance regulatory responses. The binding of a second PipX molecule per NtcA dimer, by increasing the effective concentration of NtcA-bound PipX, would raise the probability of enhanced RNAP recruitment to NtcA boxes. It might facilitate, too, the recruitment of other PipX partners, potentially further modulating transcriptional activity. Finally, given the inferred instability of free PipX molecules in *S. elongatus* [78], the NtcA site facing away from the RNAP could chaperone PipX by allowing its binding under conditions favoring PipX-NtcA complexes.

NtcA, a distinctive class II regulator of cyanobacteria working with a co-activator

Activation by a protein factor in addition to an effector small molecule, makes NtcA unique within the CRP/FNR family. Moreover, NtcA deviates from the typical behavior of class II activators [5, 80] by not interacting with the α subunit of RNAP's N-terminal domain or C-terminal domain, as shown in the structures reported by [19]. This raises the intriguing possibility that PipX might be necessary for these interactions to occur. It is worth noting that PipX could also fit without causing steric clashes into even larger complexes (Supplementary Fig. S7) mediating cooperative transcription activation by NtcA and NtcB [19], a LysR-type regulator involved in nitrite utilization in *Synechococcus* [81], thus suggesting a potential mechanism for combined regulation of certain genes that might require the coordinated action of two transcription factors and PipX, particularly under conditions of nitrogen depletion.

PipX is particularly important for activation of non-canonical NtcA-dependent promoters involved in nitrogen utilization like *glnN* [31, 55], but it also seems that most, if not all, of the large NtcA regulon would use PipX as a co-activator [24]. Therefore, co-activation by PipX appears to be globally very important for cyanobacteria, contributing to fine-tuning gene expression in response to environmental changes and to orchestrate NtcA responses to nitrogen limitation.

Our work provides new insights into transcriptional regulation within the CRP-FNR superfamily in bacteria, highlighting the role of the co-activator PipX in modulating transcription factor activity. These findings support the importance of the PipX-NtcA interaction in cyanobacterial transcriptional regulation, and raise the possibility of further co-activation mechanisms within this superfamily. While the structural details presented here offer a foundation for further studies, additional research will be necessary to determine whether similar mechanisms operate in other CRP-FNR family members.

Acknowledgements

The authors thank T. Mata for excellent technical assistance.

Author contributions: Conceptualization, V.R., J.L.L.; methodology, A.F.-N, J.L.L., P.S.; formal analysis, A.F.-N, V.R., J.L.L., S.B, P.S., A.C.; investigation, A.F.-N, J.L.L., S.B, P.S.; resources, A.F.-N, J.L.L.; writing –original draft, A.F.-N, J.L.L., V.R., A.C.; writing – review & editing, A.F.-N, V.R., J.L.L., S.B, P.S., A.C.; visualization, A.F.-N, V.R., J.L.L., S.B, P.S., A.C.; supervision, V.R., J.L.L., A.C.; project administration, V.R., J.L.L., A.C.; funding acquisition, V.R., J.L.L., A.C., S.B.

Supplementary data

Supplementary data is available at NAR online.

Conflict of interest

None declared.

Funding

Supported by grants of the Ministerio de Ciencia, Innovación y Universidades PID2020-116880GB-I00 to J.L.L.; PID2020-

118816GB-I00 and PID2023-149456NB-I00 to A.C.; and BFU2017-84264-P to V.R.; as well as Fundación Ramón Areces grant CIV20A6610 to V.R. S.B. was supported by a national grant from the Ministère de l'Enseignement Supérieur et de la Recherche Scientifique (MESR), Algeria. The Open Access publication charges for this article were assumed by the Consejo Superior de Investigaciones Científicas (CSIC) of Spain.

Data availability

Six atomic coordinate models have been deposited in the PDB with accession codes 9GUI, 9GUJ, 9GUK, 9GUG, 9GQU, and 9GUH.

References

- Körner H, Sofia HJ, Zumft WG. Phylogeny of the bacterial superfamily of Crp-Fnr transcription regulators: exploiting the metabolic spectrum by controlling alternative gene programs. *FEMS Microbiol Rev* 2003;27:559–92. [https://doi.org/10.1016/S0168-6445\(03\)00066-4](https://doi.org/10.1016/S0168-6445(03)00066-4)
- Krol E, Werel L, Essen LO *et al.* Structural and functional diversity of bacterial cyclic nucleotide perception by CRP proteins. *MicroLife* 2023;4:uqad024. <https://doi.org/10.1093/femsml/uqad024>
- Roberts MG, Dent MR, Ramos S *et al.* Probing conformational dynamics of DNA binding by CO-sensing transcription factor, CooA. *J Inorg Biochem* 2024;259:112656. <https://doi.org/10.1016/j.jinorgbio.2024.112656>
- Vega-Palas MA, Flores E, Herrero A. NtcA, a global nitrogen regulator from the cyanobacterium *Synechococcus* that belongs to the Crp family of bacterial regulators. *Mol Microbiol* 1992;6:1853–9. <https://doi.org/10.1111/j.1365-2958.1992.tb01357.x>
- Lawson CL, Swigon D, Murakami KS *et al.* Catabolite activator protein: DNA binding and transcription activation. *Curr Opin Struct Biol* 2004;14:10–20. <https://doi.org/10.1016/j.sbi.2004.01.012>
- Schultz SC, Shields GC, Steitz TA. Crystal structure of a CAP–DNA complex: the DNA is bent by 90°. *Science* 1991;253:1001–7.
- Parkinson G, Wilson C, Gunasekera A *et al.* Structure of the CAP–DNA complex at 2.5 Å resolution: a complete picture of the protein–DNA interface. *J Mol Biol* 1996;260:395–408. <https://doi.org/10.1006/jmbi.1996.0409>
- Chen S, Vojtechovsky J, Parkinson GN *et al.* Indirect readout of DNA sequence at the primary-kink site in the CAP–DNA complex: DNA binding specificity based on energetics of DNA kinking. *J Mol Biol* 2001;314:63–74. <https://doi.org/10.1006/jmbi.2001.5089>
- Chen S, Gunasekera A, Zhang X *et al.* Indirect readout of DNA sequence at the primary-kink site in the CAP–DNA complex: alteration of DNA binding specificity through alteration of DNA kinking. *J Mol Biol* 2001;314:75–82. <https://doi.org/10.1006/jmbi.2001.5090>
- Napoli AA, Lawson CL, Ebright RH *et al.* Indirect readout of DNA sequence at the primary-kink site in the CAP–DNA complex: recognition of pyrimidine–purine and purine–purine steps. *J Mol Biol* 2006;357:173–83. <https://doi.org/10.1016/j.jmb.2005.12.051>
- Benoff B, Yang H, Lawson CL *et al.* Structural basis of transcription activation: the CAP- α CTD–DNA complex. *Science* 2002;297:1562–6. <https://doi.org/10.1126/science.1076376>
- Levy C, Pike K, Heyes DJ *et al.* Molecular basis of halorespiration control by CprK, a CRP–FNR type transcriptional regulator. *Mol Microbiol* 2008;70:151–67. <https://doi.org/10.1111/j.1365-2958.2008.06399.x>
- Hall M, Grundström C, Begum A *et al.* Structural basis for glutathione-mediated activation of the virulence regulatory protein PrfA in *Listeria*. *Proc Natl Acad Sci USA* 2016;113:14733–8. <https://doi.org/10.1073/pnas.1614028114>
- Bonnet M, Kurz M, Mesa S *et al.* The structure of *Bradyrhizobium japonicum* transcription factor FixK 2 unveils sites of DNA binding and oxidation. *J Biol Chem* 2013;288:14238–46. <https://doi.org/10.1074/jbc.M113.465484>
- Werel L, Farmani N, Krol E *et al.* Structural basis of dual specificity of *Sinorhizobium meliloti* Ctr, a cAMP and cGMP receptor protein. *mBio* 2023;14:e0302822. <https://doi.org/10.1128/mbio.03028-22>
- Feng Y, Zhang Y, Ebright RH. Structural basis of transcription activation. *Science* 2016;352:1330–3. <https://doi.org/10.1126/science.aaf4417>
- Liu B, Hong C, Huang RK *et al.* Structural basis of bacterial transcription activation. *Science* 2017;358:947–51. <https://doi.org/10.1126/science.aao1923>
- Shi W, Jiang Y, Deng Y *et al.* Visualization of two architectures in class-II CAP-dependent transcription activation. *PLoS Biol* 2020;18:e3000706. <https://doi.org/10.1371/journal.pbio.3000706>
- Han S-J, Jiang Y-L, You L-L *et al.* DNA looping mediates cooperative transcription activation. *Nat Struct Mol Biol* 2024;31:293–9. <https://doi.org/10.1038/s41594-023-01149-7>
- Herrero A, Muro-Pastor AM, Flores E. Nitrogen control in cyanobacteria. *J Bacteriol* 2001;183:411–25. <https://doi.org/10.1128/JB.183.2.411-425.2001>
- Herrero A, Muro-Pastor AM, Valladares A *et al.* Cellular differentiation and the NtcA transcription factor in filamentous cyanobacteria. *FEMS Microbiol Rev* 2004;28:469–87. <https://doi.org/10.1016/j.femsre.2004.04.003>
- Su Z, Olman V, Mao F *et al.* Comparative genomics analysis of NtcA regulons in cyanobacteria: regulation of nitrogen assimilation and its coupling to photosynthesis. *Nucleic Acids Res* 2005;33:5156–71. <https://doi.org/10.1093/nar/gki817>
- Mitschke J, Vioque A, Haas F *et al.* Dynamics of transcriptional start site selection during nitrogen stress-induced cell differentiation in *Anabaena* sp. PCC7120. *Proc Natl Acad Sci USA* 2011;108:20130–35. <https://doi.org/10.1073/pnas.1112724108>
- Espinosa J, Rodríguez-Mateos F, Salinas P *et al.* PipX, the coactivator of NtcA, is a global regulator in cyanobacteria. *Proc Natl Acad Sci USA* 2014;111:E2423–30. <https://doi.org/10.1073/pnas.1404097111>
- Giner-Lamia J, Robles-Rengel R, Hernández-Prieto MA *et al.* Identification of the direct regulon of NtcA during early acclimation to nitrogen starvation in the cyanobacterium *Synechocystis* sp. PCC 6803. *Nucleic Acids Res* 2017;45:11800–20. <https://doi.org/10.1093/nar/gkx860>
- Llácer JL, Fita I, Rubio V. Arginine and nitrogen storage. *Curr Opin Struct Biol* 2008;18:673–81. <https://doi.org/10.1016/j.sbi.2008.11.002>
- Llácer JL, Espinosa J, Castells MA *et al.* Structural basis for the regulation of NtcA-dependent transcription by proteins PipX and PII. *Proc Natl Acad Sci USA* 2010;107:15397–402. <https://doi.org/10.1073/pnas.1007015107>
- Zhao M-X, Jiang Y-L, He Y-X *et al.* Structural basis for the allosteric control of the global transcription factor NtcA by the nitrogen starvation signal 2-oxoglutarate. *Proc Natl Acad Sci USA* 2010;107:12487–92. <https://doi.org/10.1073/pnas.1001556107>
- Burillo S, Luque I, Fuentes I. Interactions between the nitrogen signal transduction protein PII and N-acetyl glutamate kinase in organisms that perform oxygenic photosynthesis. *J Bacteriol* 2004;186:3346–54. <https://doi.org/10.1128/JB.186.11.3346-3354.2004>
- Labella JI, Cantos R, Salinas P *et al.* Distinctive features of PipX, a unique signaling protein of cyanobacteria. *Life* 2020;10:79. <https://doi.org/10.3390/life10060079>
- Espinosa J, Forchhammer K, Burillo S *et al.* Interaction network in cyanobacterial nitrogen regulation: PipX, a protein that interacts in a 2-oxoglutarate dependent manner with PII and NtcA. *Mol*

- Microbiol* 2006;61:457–69.
<https://doi.org/10.1111/j.1365-2958.2006.05231.x>
32. Labella JI, Obrebska A, Espinosa J *et al.* Expanding the cyanobacterial nitrogen regulatory network: the GntR-like regulator PlmA interacts with the PII–PipX complex. *Front Microbiol* 2016;7:1677.
<https://doi.org/10.3389/fmicb.2016.01677>
 33. Labella JI, Cantos R, Espinosa J *et al.* PipY, a member of the conserved COG0325 family of PLP-binding proteins, expands the cyanobacterial nitrogen regulatory network. *Front Microbiol* 2017;8:1244. <https://doi.org/10.3389/fmicb.2017.01244>
 34. Forcada-Nadal A, Ll  cer JL, Contreras A *et al.* The PII–NAGK–PipX–NtcA regulatory axis of cyanobacteria: a tale of changing partners, allosteric effectors and non-covalent interactions. *Front Mol Biosci* 2018;5:91.
<https://doi.org/10.3389/fmolb.2018.00091>
 35. Luque I, Flores E, Herrero A. Molecular mechanism for the operation of nitrogen control in cyanobacteria. *EMBO J* 1994;13:2862–9.
<https://doi.org/10.1002/j.1460-2075.1994.tb06580.x>
 36. Collaborative Computational Project, Number 4 The CCP4 suite: programs for protein crystallography. *Acta Crystallogr D Biol Crystallogr* 1994;50:760–3.
<https://doi.org/10.1107/S0907444994003112>
 37. Kabsch W. XDS. *Acta Crystallogr D Biol Crystallogr* 2010;66:125–32. <https://doi.org/10.1107/S0907444909047337>
 38. Vagin A, Teplyakov A. Molecular replacement with MOLREP. *Acta Crystallogr D Biol Crystallogr* 2010;66:22–5.
<https://doi.org/10.1107/S0907444909042589>
 39. Murshudov GN, Skub  k P, Lebedev AA *et al.* REFMAC 5 for the refinement of macromolecular crystal structures. *Acta Crystallogr D Biol Crystallogr* 2011;67:355–67.
<https://doi.org/10.1107/S0907444911001314>
 40. Cowtan K. Recent developments in classical density modification. *Acta Crystallogr D Biol Crystallogr* 2010;66:470–8.
<https://doi.org/10.1107/S090744490903947X>
 41. Emsley P, Lohkamp B, Scott WG *et al.* Features and development of Coot. *Acta Crystallogr D Biol Crystallogr* 2010;66:486–501.
<https://doi.org/10.1107/S0907444910007493>
 42. Afonine PV, Poon BK, Read RJ *et al.* Real-space refinement in PHENIX for cryo-EM and crystallography. *Acta Crystallogr D Struct Biol* 2018;74:531–44.
<https://doi.org/10.1107/S2059798318006551>
 43. Winn MD, Isupov MN, Murshudov GN. Use of TLS parameters to model anisotropic displacements in macromolecular refinement. *Acta Crystallogr D Biol Crystallogr* 2001;57:122–33.
<https://doi.org/10.1107/S0907444900014736>
 44. Painter J, Merritt EA. Optimal description of a protein structure in terms of multiple groups undergoing TLS motion. *Acta Crystallogr D Biol Crystallogr* 2006;62:439–50.
<https://doi.org/10.1107/S0907444906005270>
 45. Williams CJ, Headd JJ, Moriarty NW *et al.* MolProbity: more and better reference data for improved all-atom structure validation. *Protein Sci* 2018;27:293–315. <https://doi.org/10.1002/pro.3330>
 46. McCoy AJ, Grosse-Kunstleve RW, Adams PD *et al.* Phaser crystallographic software. *J Appl Crystallogr* 2007;40:658–74.
<https://doi.org/10.1107/S0021889807021206>
 47. Krissinel E, Henrick K. Inference of macromolecular assemblies from crystalline state. *J Mol Biol* 2007;372:774–97.
<https://doi.org/10.1016/j.jmb.2007.05.022>
 48. Sambrook J, Fritsch ER, Maniatis T. *Molecular Cloning: A Laboratory Manual*, 2nd edn. Cold Spring Harbor, NY: Cold Spring Harbor Laboratory Press, 1989.
 49. Vedadi M, Niesen FH, Allali-Hassani A *et al.* Chemical screening methods to identify ligands that promote protein stability, protein crystallization, and structure determination. *Proc Natl Acad Sci USA* 2006;103:15835–40.
<https://doi.org/10.1073/pnas.0605224103>
 50. Bradford MM. A rapid and sensitive method for the quantitation of microgram quantities of protein utilizing the principle of protein-dye binding. *Anal Biochem* 1976;72:248–54.
[https://doi.org/10.1016/0003-2697\(76\)90527-3](https://doi.org/10.1016/0003-2697(76)90527-3)
 51. Sievers F, Higgins DG. Clustal Omega for making accurate alignments of many protein sequences. *Protein Sci* 2018;27:135–45. <https://doi.org/10.1002/pro.3290>
 52. Krissinel E, Henrick K. Secondary-structure matching (SSM), a new tool for fast protein structure alignment in three dimensions. *Acta Crystallogr D Biol Crystallogr* 2004;60:2256–68.
<https://doi.org/10.1107/S0907444904026460>
 53. Zheng G, Lu X-J, Olson WK. Web 3DNA—a web server for the analysis, reconstruction, and visualization of three-dimensional nucleic-acid structures. *Nucleic Acids Res* 2009;37:W240–6.
<https://doi.org/10.1093/nar/gkp358>
 54. Reyes JC, Muro-Pastor MI, Florencio FJ. Transcription of glutamine synthetase genes (*glnA* and *glnN*) from the cyanobacterium *Synechocystis* sp. strain PCC 6803 is differently regulated in response to nitrogen availability. *J Bacteriol* 1997;179:2678–89.
<https://doi.org/10.1128/jb.179.8.2678-2689.1997>
 55. Forcada-Nadal A, Forchhammer K, Rubio V. SPR analysis of promoter binding of *Synechocystis* PCC6803 transcription factors NtcA and CRP suggests cross-talk and sheds light on regulation by effector molecules. *FEBS Lett* 2014;588:2270–6.
<https://doi.org/10.1016/j.febslet.2014.05.010>
 56. Jiang F, Wis  n S, Widersten M *et al.* Examination of the transcription factor NtcA-binding motif by *in vitro* selection of DNA sequences from a random library. *J Mol Biol* 2000;301:783–93. <https://doi.org/10.1006/jmbi.2000.4000>
 57. V  zquez-Berm  dez MF, Flores E, Herrero A. Analysis of binding sites for the nitrogen-control transcription factor NtcA in the promoters of *Synechococcus* nitrogen-regulated genes. *Biochim Biophys Acta* 2002;1578:95–8.
[https://doi.org/10.1016/S0167-4781\(02\)00506-7](https://doi.org/10.1016/S0167-4781(02)00506-7)
 58. Forcada-Nadal A, Palomino-Sch  tzlein M, Neira JL *et al.* The PipX protein, when not bound to its targets, has its signaling C-terminal helix in a flexed conformation. *Biochemistry* 2017;56:3211–24. <https://doi.org/10.1021/acs.biochem.7b00230>
 59. Karimova G, Pidoux J, Ullmann A *et al.* A bacterial two-hybrid system based on a reconstituted signal transduction pathway. *Proc Natl Acad Sci USA* 1998;95:5752–6.
<https://doi.org/10.1073/pnas.95.10.5752>
 60. Battesti A, Bouveret E. The bacterial two-hybrid system based on adenylate cyclase reconstitution in *Escherichia coli*. *Methods* 2012;58:325–34. <https://doi.org/10.1016/j.ymeth.2012.07.018>
 61. Jerez C, Salinas P, Llop A *et al.* Regulatory connections between the cyanobacterial factor PipX and the ribosome assembly GTPase EngA. *Front Microbiol* 2021;12:781760.
<https://doi.org/10.3389/fmicb.2021.781760>
 62. Salinas P, Bibak S, Cantos R *et al.* Studies on the PII–PipX–NtcA regulatory axis of cyanobacteria provide novel insights into the advantages and limitations of two-hybrid systems for protein interactions. *Int J Mol Sci* 2024;25:5429.
<https://doi.org/10.3390/ijms25105429>
 63. Bell A, Busby S. Location and orientation of an activating region in the *Escherichia coli* transcription factor, FNR. *Mol Microbiol* 1994;11:383–90.
<https://doi.org/10.1111/j.1365-2958.1994.tb00318.x>
 64. Leduc J, Thorsteinsson MV, Gaal T *et al.* Mapping CoaA-RNA polymerase interactions: identification of activating regions 2 and 3 in CoaA, the CO-sensing transcriptional activator. *J Biol Chem* 2001;276:39968–73. <https://doi.org/10.1074/jbc.M105758200>
 65. Popovych N, Tzeng S-R, Tonelli M *et al.* Structural basis for cAMP-mediated allosteric control of the catabolite activator protein. *Proc Natl Acad Sci USA* 2009;106:6927–32.
<https://doi.org/10.1073/pnas.0900595106>
 66. Sharma H, Yu S, Kong J *et al.* Structure of apo-CAP reveals that large conformational changes are necessary for DNA binding.

- Proc Natl Acad Sci USA* 2009;106:16604–9. <https://doi.org/10.1073/pnas.0908380106>
67. Gallagher DT, Smith N, Kim SK *et al.* Profound asymmetry in the structure of the cAMP-free cAMP receptor protein (CRP) from *Mycobacterium tuberculosis*. *J Biol Chem* 2009;284:8228–32. <https://doi.org/10.1074/jbc.C800215200>
 68. Kumar P, Joshi DC, Akif M *et al.* Mapping conformational transitions in cyclic AMP receptor protein: crystal structure and normal-mode analysis of *Mycobacterium tuberculosis* apo-cAMP receptor protein. *Biophys J* 2010;98:305–14. <https://doi.org/10.1016/j.bpj.2009.10.016>
 69. Lanzilotta WN, Schuller DJ, Thorsteinsson MV *et al.* Structure of the CO sensing transcription activator CooA. *Nat Struct Biol* 2000;7:876–80.
 70. Townsend PD, Jungwirth B, Pojer F *et al.* The crystal structures of apo and cAMP-bound GlxR from *Corynebacterium glutamicum* reveal structural and dynamic changes upon cAMP binding in CRP/FNR family transcription factors. *PLoS One* 2014;9:e113265. <https://doi.org/10.1371/journal.pone.0113265>
 71. Seok S-H, Im H, Won H-S *et al.* Structures of inactive CRP species reveal the atomic details of the allosteric transition that discriminates cyclic nucleotide second messengers. *Acta Crystallogr D Biol Crystallogr* 2014;70:1726–42. <https://doi.org/10.1107/S139900471400724X>
 72. Kuchinskas M, Li H, Conrad M *et al.* The role of the DNA-binding domains in CooA activation. *Biochemistry* 2006;45:7148–53. <https://doi.org/10.1021/bi052609o>
 73. Mazon H, Gábor K, Leys D *et al.* Transcriptional activation by CprK1 is regulated by protein structural changes induced by effector binding and redox state. *J Biol Chem* 2007;282:11281–90. <https://doi.org/10.1074/jbc.M611177200>
 74. Agari Y, Kashiwara A, Yokoyama S *et al.* Global gene expression mediated by *Thermus thermophilus* SdrP, a CRP/FNR family transcriptional regulator. *Mol Microbiol* 2008;70:60–75. <https://doi.org/10.1111/j.1365-2958.2008.06388.x>
 75. Volbeda A, Darnault C, Renoux O *et al.* The crystal structure of the global anaerobic transcriptional regulator FNR explains its extremely fine-tuned monomer-dimer equilibrium. *Sci Adv* 2015;1:1501086. <https://doi.org/10.1126/sciadv.1501086>
 76. Valladares A, Flores E, Herrero A. Transcription activation by NtcA and 2-oxoglutarate of three genes involved in heterocyst differentiation in the cyanobacterium *Anabaena sp.* strain PCC 7120. *J Bacteriol* 2008;190:6126–33. <https://doi.org/10.1128/JB.00787-08>
 77. Llop A, Bibak S, Cantos R *et al.* The ribosome assembly GTPase EngA is involved in redox signaling in cyanobacteria. *Front Microbiol* 2023;14:1242616. <https://doi.org/10.3389/fmicb.2023.1242616>
 78. Llop A, Tremiño L, Cantos R *et al.* The signal transduction protein PII controls the levels of the cyanobacterial protein PipX. *Microorganisms* 2023;11:2379. <https://doi.org/10.3390/microorganisms11102379>
 79. Jerez C, Llop A, Salinas P *et al.* Analysing the cyanobacterial PipX interaction network using NanoBiT complementation in *Synechococcus elongatus* PCC7942. *Int J Mol Sci* 2024;25:4702. <https://doi.org/10.3390/ijms25094702>
 80. Busby S, Ebright RH. Transcription activation by catabolite activator protein (CAP). *J Mol Biol* 1999;293:199–213. <https://doi.org/10.1006/jmbi.1999.3161>
 81. Aichi M, Omata T. Involvement of NtcB, a LysR family transcription factor, in nitrite activation of the nitrate assimilation operon in the cyanobacterium *Synechococcus sp.* strain PCC 7942. *J Bacteriol* 1997;179:4671–5. <https://doi.org/10.1128/jb.179.15.4671-4675.1997>